Size-resolved, quantitative evaluation of the magnetic mineralogy of airborne brake-wear particulate emissions

Tomasz Gonet[a,*], Barbara A. Maher[a], Ilona Nyirő-Kósa[b], Mihály Pósfai[c], Miroslav Vaculík[d,e], Jana Kukutschová[e,f]

[a]Centre for Environmental Magnetism & Palaeomagnetism, Lancaster Environment Centre, Lancaster University, Lancaster LA1 4YQ, United Kingdom

[b]MTA-PE Air Chemistry Research Group, 10 Egyetem Street, H-8200 Veszprém, Hungary

[c]Research Institute of Biomolecular and Chemical Engineering, University of Pannonia, Veszprém, H8200 Hungary

[d]Nanotechnology Centre, VSB-Technical University of Ostrava, 708 00 Ostrava-Poruba, Czech Republic

[e]Centre for Advanced Innovative Technologies, VSB-Technical University of Ostrava, 708 00 Ostrava-Poruba, Czech Republic

[f]Faculty of Materials Science and Technology, VSB-Technical University of Ostrava, 708 00 Ostrava, Czech Republic

*Corresponding author: Tomasz Gonet; t.gonet@lancaster.ac.uk; Lancaster Environment Centre, Lancaster University, Farrer Avenue, Lancaster University, Lancaster LA1 4YQ

ABSTRACT:

Exposure to particulate air pollution has been associated with a variety of respiratory, cardiovascular and neurological problems, resulting in increased morbidity and mortality worldwide. Brake-wear emissions are one of the major sources of metal-rich airborne particulate pollution in roadside environments. Of potentially bioreactive metals, Fe (especially in its ferrous form, Fe^{2+}) might play a specific role in both neurological and cardiovascular impairments. Here, we collected brake-wear particulate emissions using a full-scale brake dynamometer, and used a combination of magnetic measurements and electron microscopy to make quantitative evaluation of the magnetic composition and particle size of airborne emissions originating from passenger car brake systems. Our results show that the concentrations of Fe-rich magnetic grains in airborne brake-wear emissions are very high (i.e., ~100 – 10000 × higher), compared to other types of particulate pollutants produced in most urban environments. From magnetic component analysis, the average magnetite mass concentration in total PM_{10} of brake emissions is ~20.2 wt.% and metallic Fe ~1.6 wt.%. Most brake-wear airborne particles (> 99% of particle number concentration) are smaller than 200 nm. Using low-temperature magnetic measurements, we observed a strong superparamagnetic signal (indicative of ultrafine magnetic particles, < ~30 nm) for all of the analysed size fractions of airborne brake-wear particles. Transmission electron microscopy independently shows that even the larger size fractions of airborne brake-wear emissions dominantly comprise agglomerates of ultrafine (< 100 nm) particles (UFPs). Such UFPs likely pose a threat to neuronal and cardiovascular health after inhalation and/or ingestion. The observed abundance of ultrafine magnetite particles (estimated to constitute ~7.6 wt.% of $PM_{0.2}$) might be especially hazardous to the brain, contributing both to microglial inflammatory action and excess generation of reactive oxygen species.

KEYWORDS: air pollution, brake wear, particulate matter, magnetite, neurodegeneration

LIST OF ABBREVIATIONS:

ARM – anhysteretic remanent magnetisation

BF – bright field

EDS – energy dispersive X-ray spectrometry

FFT – fast Fourier transform

FORC – first order reversal curve

HAADF – high angle annular dark-field mode of transmission electron microscopy (TEM)

HRTEM – high-resolution transmission electron microscopy (TEM)

IRM – isothermal remanence magnetisation, or magnetic remanence

$\kappa_{fd\%}$ - frequency dependence of magnetic susceptibility

MDF_{IRM} – median destructive field of IRM

PAHs – polycyclic aromatic hydrocarbons

PM – particulate matter

PM_{10} – particulate matter with an aerodynamic diameter < 10 μm

$PM_{2.5}$ – particulate matter with an aerodynamic diameter < 2.5 μm

$PM_{0.2}$ – particulate matter with an aerodynamic diameter < 0.2 μm

PNC – particle number concentration

PSD – particle size distribution

ROS – reactive oxygen species

SAED – selected-area electron diffraction

SE – secondary electrons

SEM – scanning electron microscopy

STEM – scanning transmission electron microscopy

SD – single domain

SP – superparamagnetic

T_M – temperature of the Morin transition in haematite

T_V – temperature of the Verwey transition in magnetite

TEM – transmission electron microscopy

UFPs – ultrafine particles

XRD – X-ray diffraction

GRAPHICAL ABSTRACT

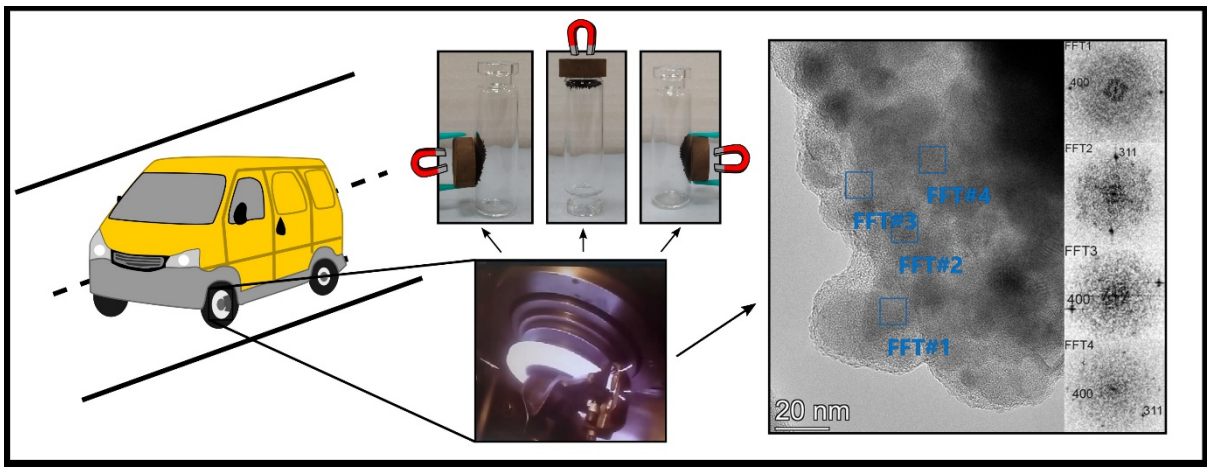

Introduction

Exposure to airborne particulate matter (PM) has been associated with both acute and chronic health problems. Coarse (10 – 2.5 μm), fine (2.5 – 0.1 μm) and ultrafine (< 0.1 μm) particles have been linked to impairment of pulmonary, cardiovascular and neurological health (Calderón-Garcidueñas *et al*., 2002; Pope & Dockery, 2006; Hoek *et al*., 2013; Beelen *et al*., 2014; Weichenthal *et al*., 2017; Peters *et al*., 2019; Maher *et al.*, 2020, Shi et al., 2020). For example, epidemiological studies have shown a link between living close to heavy traffic (and consequently, chronic exposure to raised airborne PM concentrations) with higher incidence of dementia (Jung *et al*., 2015; Wu *et al*., 2015; Oudin *et al*., 2016; Chen *et al*., 2017), and cognitive and behavioural deficits (Suglia *et al*., 2007; Chen & Schwartz, 2009; Sunyer *et al*., 2015; Zhang *et al*., 2018; Calderón-Garcidueñas *et al*., 2019a; Iaccarino *et al*., 2020). Exposure to PM is also linked to pre-term birth and low birth weight (e.g. Stieb *et al*., 2012; Lamichhane *et al*., 2015; Li *et al*., 2017).

Ultrafine particles (UFPs) might be especially hazardous to human health for several reasons. They (i) are abundant in the urban air (Putaud *et al*., 2010; Sanderson *et al*., 2014; Yang *et al*., 2016); (ii) can be suspended in the atmosphere for longer and consequently, transported over greater distances, compared to coarse particles; (iii) are able to penetrate easily into the indoor environment; (iv) have the ability to reach almost all organs in the human body, including the liver (Oberdörster *et al*., 2002; Miller *et al*., 2017), placenta (Bové *et al*., 2019; Liu *et al*., 2021) and amniotic fluid (Barošová *et al*., 2015), heart (Calderón-Garcidueñas *et al*., 2019b; Maher *et al*., 2020), and central nervous system (Tjälve *et al*., 1996; Oberdörster *et al.*, 2004; Elder *et al*., 2006; Geiser & Kreyling *et al*., 2010; Maher *et al*., 2016); (v) have a larger surface area per unit mass, compared to coarse particles; and (vi) can be highly bioreactive (Donaldson *et al*., 2001; Nel *et al*., 2006; Maher *et al*., 2016).

Exposure to Fe-bearing UFPs might play a specific role in adverse health effects (Maher *et* al., 2016, 2020). Labile, bioreactive Fe^{2+} (a specific component within magnetite (Fe_3O_4 = $FeO{\cdot}Fe_2O_3$, a mixed Fe^{2+}/Fe^{3+} oxide), for example), can be toxic to living cells; it can catalyse excess production of reactive oxygen species (ROS) and has been linked with neurodegenerative changes similar to those occurring in Alzheimer's disease (Smith *et al*., 1997; Wu *et al*., 2013; Coccini *et al*., 2017; Maher, 2019). Fe-bearing UFPs may be toxic on their own but also often co-associate with other transition and heavy metals, including Cr, Cu, Mn, Ni, Pb, Zn (Spassov *et al*., 2004; Chen *et al*., 2006; Kim *et al*., 2007; Maher *et al*., 2016; Yang *et al*., 2016; Hofman *et al*., 2020) and organic species, including polycyclic aromatic hydrocarbons (PAHs) (Lehndorff & Schwark, 2004; Halsall *et al*., 2008).

In the urban environment, a great variety of both vehicular and non-vehicular sources of Fe-bearing UFPs has been identified, including exhaust emissions, brake wear, tyre wear, resuspension

of roadside dust, underground, rail and tram systems, aircraft and shipping emissions, welding fumes, waste incineration, biomass burning, construction, demolition, power plants and cigarette smoking (e.g., Thorpe & Harrison, 2008; Salma *et al*., 2009; Kumar *et al*., 2013; Gonet & Maher, 2019). However, estimation of the contributions made by specific sources to total airborne PM or PNC (particle number concentration) has proved challenging, and variable between different studies (e.g. Viana *et al*., 2008; Bukowiecki *et al*., 2009a; Harrison *et al*., 2011, 2012; Lawrence *et al*., 2013; Beddows *et al*., 2015; Crilley *et al*., 2017; Conte & Contini, 2019). Although the concentrations of gaseous and particulate engine exhaust emissions have been decreasing notably in the last 20 years, due to increasingly stringent legislation, non-exhaust emissions are currently unregulated and presently constitute a similar or even higher proportion of urban PM_{10} (PM with an aerodynamic diameter < 10 μm) concentrations, compared to exhaust emissions (e.g. Lawrence et al., 2013; Denier van der Gon et al., 2018; Conte & Contini, 2019).

One of the major sources of airborne, Fe-bearing UFPs in the roadside environment is brake emissions (Gonet & Maher, 2019). Although source apportionment estimates differ, brake-wear PM has been reported to contribute more to total PM_{10} mass (~11% - 21%; Bukowiecki *et al*., 2009a; Lawrence *et al*., 2013) than to particle number (~1.7%; Harrison *et al*., 2011) at the roadside.

The emission of solid (non-volatile) brake-derived components depends on the braking conditions but in real-world conditions, they usually exceed 75 wt.% of total brake emissions (Sanders *et al*., 2002; Roubicek *et al*., 2008). Fe is frequently the dominant metal in non-volatile brake-wear PM (arising from conventional low-metallic brake pads and cast iron discs), often constituting ~50% of the total mass of particles emitted from brake systems (Sanders *et al*., 2003; Adachi & Tainosho, 2004; Kukutschová *et al*., 2011). The number-normalised particle size distribution (PSD) of brake emissions is usually dominated by fine and ultrafine fractions, with UFPs (< 0.1 μm) constituting up to 95% of total particle number (Garg *et al*., 2000; Sanders *et al*., 2003; Verma *et al*., 2016). Since UFPs constitute the vast majority of brake-wear particle numbers, and Fe is the dominant metal of those emissions, brake-derived dust might thus be a major source of urban airborne Fe-bearing UFPs (Gonet & Maher, 2019).

Fe in brake emissions has been found in various forms: magnetite (Fe_3O_4), maghemite (γ-Fe_2O_3), haematite (α-Fe_2O_3), wüstite (FeO) and metallic Fe (α-Fe) (e.g., Kukutschová & Filip, 2018). Little attention has yet been paid to the mass concentrations of specific magnetic phases/minerals. In terms of potential association with neurodegeneration and Alzheimer's disease, the oxidation state of Fe (e.g., metallic Fe, Fe^0; ferrous Fe, Fe^{2+}; ferric Fe, Fe^{3+}) may be critical (Smith *et al*., 1997; Collingwood & Dobson, 2006; Castellani *et al*., 2007; Pankhurst *et al*., 2008; Plascencia-Villa *et al*., 2016; Maher *et*

al., 2016; Maher, 2019). Hence, quantitative evaluation of the magnetic mineralogy of roadside, traffic-derived UFPs, and especially, of the concentration and particle size distribution of Fe^{2+}-bearing magnetite, may be particularly important in the context of human health hazard.

Here, we use a combination of magnetic component analysis of room- and low-temperature magnetic measurements and scanning (SEM) and transmission (TEM) electron microscopy to obtain quantitative evaluation of the mineralogy and particle size of magnetically-ordered particles within airborne PM emissions originating from automotive brake systems.

Methods

Brake-wear generation, braking cycle and particulate matter sampling

Brake-wear emission tests were performed using a full-scale brake dynamometer (Link M2800) at VŠB – Technical University of Ostrava, Czech Republic. The dynamometer was equipped with an environmental chamber, with cooling airflow of 2500 m^3/h around the brake system. Commercially available low-metallic brake pads, a cast iron brake disc and hardware of a mid-size passenger car were used, during the ISO26867 brake cycle simulating friction behaviour at different speeds and brake pressures. The composition of the brake pad was analysed using X-ray diffraction (XRD). The dynamometer test was conducted 4 times and results for the 4 sets of collected samples were averaged; i.e. the particle size distributions (Fig. 1A), IRMs (Fig. 1B), magnetic component analysis, and estimated mass concentrations of magnetite, metallic Fe and haematite. The same brake pad/disc system was used 4 times (each time a new set of brake pads was used).

A Dekati ELPI+ impactor was used to collect brake-derived primary particles directly in the dynamometer chamber, on Al foils, in 14 stages (size fractions), from 0.016 µm to 10 µm (Table SI 1). Additionally, the non-airborne fraction, swept from the floor of the dynamometer chamber after the test cycle, was also collected (hereafter called 'non-airborne brake emissions').

All Al foils were weighed before and after the dynamometer tests, and the difference treated as the mass of the collected brake-derived particles. The mass measurements were made using a Mettler Toledo XP6U/M ultra-micro balance with accuracy of 0.1 µg.

Number-normalised PSD was estimated based on the masses of particles collected on each foil and average effective density of airborne brake-derived particles emitted by a low-metallic brake pad (0.75 g/cm^3), from Nosko & Olofsson (2017a).

144 Magnetic measurements and electron microscopy

145 Brake-wear emissions were analysed by magnetic remanence measurements conducted at room
146 temperature at the Centre for Environmental Magnetism and Palaeomagnetism, Lancaster University,
147 UK; and at low temperature (down to 77 K) at the Centre for Science at Extreme Conditions, University
148 of Edinburgh, UK.

149 To obtain independent information on the composition, structure, morphology and particle size
150 of the brake-wear particles, we used scanning (SEM) and transmission (TEM) electron microscopy to
151 image and analyse the particles directly at the Research Institute of Biomolecular and Chemical
152 Engineering, University of Pannonia, Veszprém, Hungary. Two units of the aluminium foil with the
153 deposited particles (stage 10 with nominal particle size of 1.6 µm and stage 11 with nominal particle
154 size of 2.5 µm) were analysed with SEM and TEM. The particle size given by the manufacturer (DEKATI)
155 is an average size of particles collected by a certain stage (size fraction). The actual size distribution of
156 the particles collected by each stage can vary across a wide range (e.g. Pagels *et al*., 2005; Noël *et al*.,
157 2013), e.g. for the nominal size fraction of 3.0 µm, the particle size ranges from 0.2 µm up to even >10
158 µm (Pagels *et al*., 2005).

159 Details of all of the sample preparation and analytical procedures are provided in the Supporting
160 Information (SI 2).

161 # Results

162 Particle size distribution

163 The particle size distribution (PSD) of the airborne brake-wear emissions is shown in Figure 1A in
164 terms of both mass and number. UFPs (< 0.1 µm) contribute very little to the mass-based metrics, but
165 account for > 99% of the total number of emitted brake-derived particles. Conversely, the mass-
166 normalised PSD is dominated (> 90%) by particles bigger than 1 µm (Fig. 1A). Similar results have been
167 obtained elsewhere (Garg *et al*., 2000; Verma *et al*., 2016; Nosko & Olofsson, 2017b).

168

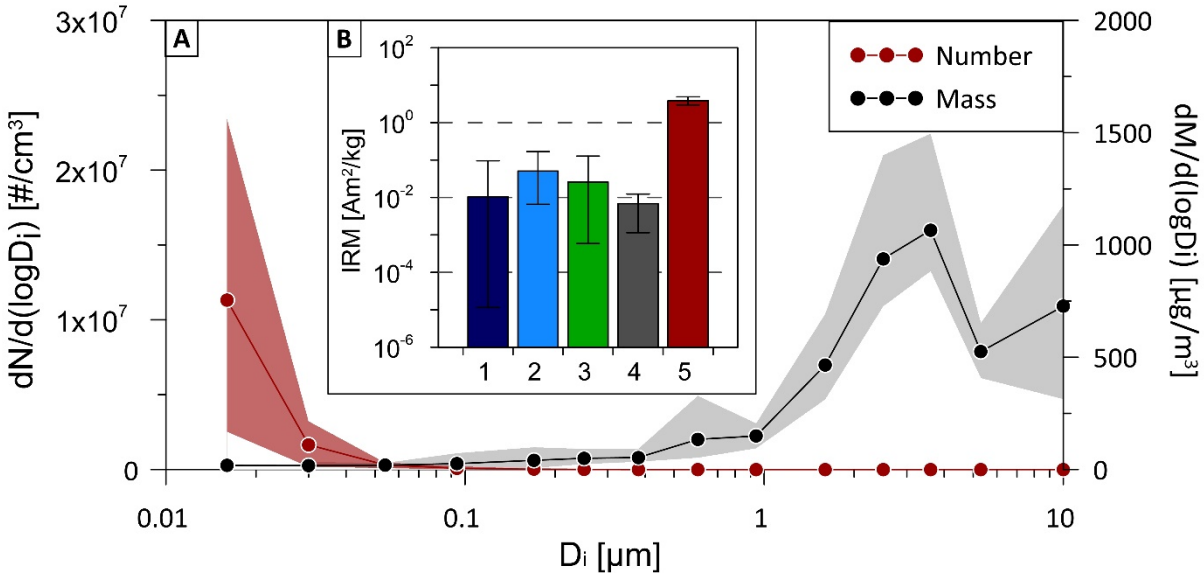

170 **Figure 1.** (A) Average mass- and number-normalised particle size distributions for the analysed brake
171 emissions. M – particle mass; N – particle number; D_i – average grain size; the shaded areas represent
172 the minimum and maximum levels of particle mass/number observed in the 4 dynamometer
173 experiments. (B) Isothermal remanent magnetisation (IRM), imparted at 1 T at room temperature at
174 the Centre for Environmental Magnetism & Palaeomagnetism, Lancaster University, for (1) outdoor
175 PM sources (Hansard *et al*., 2012), (2) roadside PM in Lancaster (Halsall *et al*., 2008; Gonet *et al*., 2021),
176 (3) indoor PM (Halsall *et al*., 2008), (4) engine exhaust PM (Gonet *et al*., 2021) and (5) airborne brake-
177 wear PM (low-metallic brake pad/cast iron disc; this study).

178

179 Magnetic content of brake emissions

180 Figure 1B shows the room-temperature magnetic remanence (IRM, acquired at 1 T) for various
181 types of PM emissions measured in our laboratory, including indoor and outdoor PM, exhaust
182 emissions and brake wear (Gonet & Maher, 2019; Gonet *et al.*, 2021). The IRM of a material depends
183 on the concentration of magnetic grains, and their magnetic mineralogy and/or grain size distribution.
184 Here, our analysed range of airborne particles display IRM values of between ~$0.01 \cdot 10^{-3}$ Am^2/kg and
185 ~$95.8 \cdot 10^{-3}$ Am^2/kg for outdoor PM sources; between ~$0.06 \cdot 10^{-3}$ Am^2/kg and ~$8.32 \cdot 10^{-3}$ Am^2/kg for
186 indoor PM sources; and for engine exhaust emissions between ~$5.1 \cdot 10^{-3}$ Am^2/kg (gasoline emissions)
187 and ~$8.6 \cdot 10^{-3}$ Am^2/kg (diesel emissions).

188 In stark contrast, the IRM values for our brake-wear particles are 100 – 10000 times higher;
189 reaching average values of ~$3383 \cdot 10^{-3}$ Am^2/kg for the airborne fraction (PM_{10}) and ~$8891 \cdot 10^{-3}$ Am^2/kg
190 for the non-airborne fraction. IRM values for airborne brake emissions were similar for all 4 sampling
191 cycles, varying between $2963 \cdot 10^{-3}$ Am^2/kg and $3800 \cdot 10^{-3}$ Am^2/kg.

In comparison, IRMs for roadside PM, both the airborne fraction (pumped air samples, Lancaster, U.K.; Halsall *et al*., 2008) and total roadside dust (dust swept from roadside surfaces), fall in the lower range between exhaust emissions (and other PM sources) and brake emissions (low-metallic brake pad/cast iron disc), reaching levels of ~66.5·10^{-3} Am^2/kg and ~34.8·10^{-3} Am^2/kg for airborne and total roadside PM, respectively (cf. Fig. 1B).

For the size-fractionated brake emissions (Figure 2), IRM decreases with decreasing particle size from >3000·10^{-3} Am^2/kg for particle sizes ~1.6 – 10 µm (stages 10 – 14) to <500·10^{-3} Am^2/kg for particle sizes ~0.016 – 0.054 µm (stages 1 – 3). This trend most probably reflects lower concentrations of both magnetite and magnetic Fe (cf. Fig. SI 2.4 and discussion on the mass concentrations of magnetite and metallic Fe with particle size in the Discussion section).

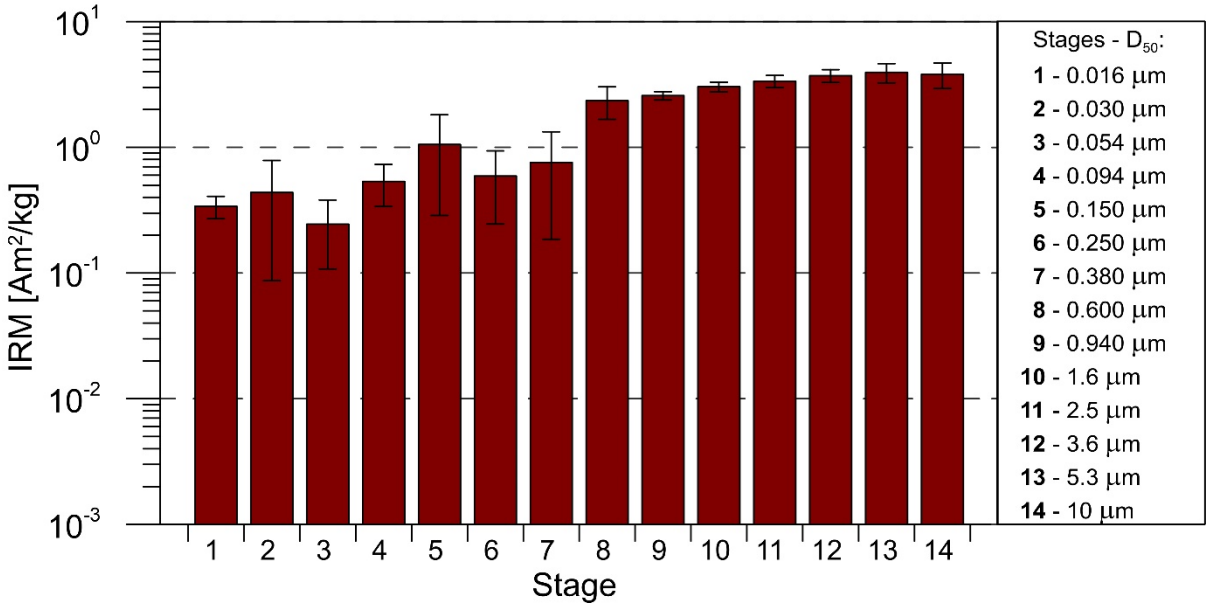

Figure 2. Average isothermal remanent magnetisation (IRM), imparted at 1 T at room temperature, for size-fractionated brake-wear emissions from low-metallic brake pads collected in 4 dynamometer sampling cycles.

Magnetic component unmixing

Each magnetic phase is characterised by several parameters, including the median destructive field of the IRM (MDF_{IRM}, indicating how easily a sample can be demagnetised); and a dispersion parameter (describing the level of scattering around the mean MDF_{IRM}). Detailed AF demagnetisation of IRM allowed identification of 3 magnetic components (C1, C2 and C3) in the brake emissions (SI 2). Two of these identified components are magnetically 'soft', i.e., they demagnetise at low AF values (MDF_{IRM} of 12 mT and 28 mT for C1 and C3, respectively), and one (C2) is magnetically 'hard', having

distinctly higher MDF_{IRM} (81 mT). The dispersion parameter is lowest for C2 (~0.16), higher for C3 (~0.31) and highest for C1 (~0.40). On average, magnetic component C1 contributes ~37.6% to total IRM, component C2 accounts for ~5.6%, and C3 for ~56.8% of total IRM (Table SI 2.1). These 'magnetic' contributions can be used for estimation of mass concentrations of specific magnetic minerals/phases, i.e. magnetite, haematite and metallic Fe (see Discussion).

Low-temperature magnetic measurements

Our low-temperature magnetic remanence measurements identify, first, magnetic transitions diagnostic of different minerals and particle sizes (see also SI 5). Specifically, the Morin transition, a first order magnetic transition in haematite, is visible at ~210-220 K, and the Verwey transition, diagnostic of the presence of magnetite, is seen at ~100 – 150K (Fig. 3A). The Verwey transition for the measured brake-wear samples is not sharp, reflecting either very small grain size (close to the stable single domain/superparamagnetic boundary, ~30 nm), non-stoichiometry of magnetite, and/or substitutions of Fe by other metals (e.g. Özdemir *et al*., 1993). A relatively low Verwey transition temperature (T_V < 100K) also suggests the presence of ultrafine grains of magnetite/maghemite (Özdemir & Dunlop, 2010; Özdemir et al., 1993).

The low-temperature measurements also show sharp increases in magnetic remanence with cooling (Fig. 3B), reflecting the magnetic 'blocking in' of ultrafine (< ~30 nm), superparamagnetic (SP) grains, which were magnetically unstable at room temperature through thermal agitation. To quantify the SP contribution, we estimated ΔM (Fig. 3B), compared to the total IRM (at 5 T and 77 K), for the selected samples. Counter-intuitively, ΔM seems to decrease with decreasing particle size, reaching 44% - 46% for stages 13, 11 and 7 (~5.3 µm, ~2.5 µm and ~0.380 µm, respectively), and declining to 32% for stage 3 (~0.054 µm) and 28% for stage 1 (~0.016 µm). This behaviour might reflect: (1) agglomeration of SP grains and/or their adherence to bigger particles, and hence their effective assignment as larger particles (i.e., collected in the larger particle stages) by the impactor, and/or (2) the presence of SP, oxidised rims around larger magnetic grains. The latter has been suggested by Özdemir *et al*. (1993), Sagnotti *et al*. (2009) and Sagnotti & Winkler (2012).

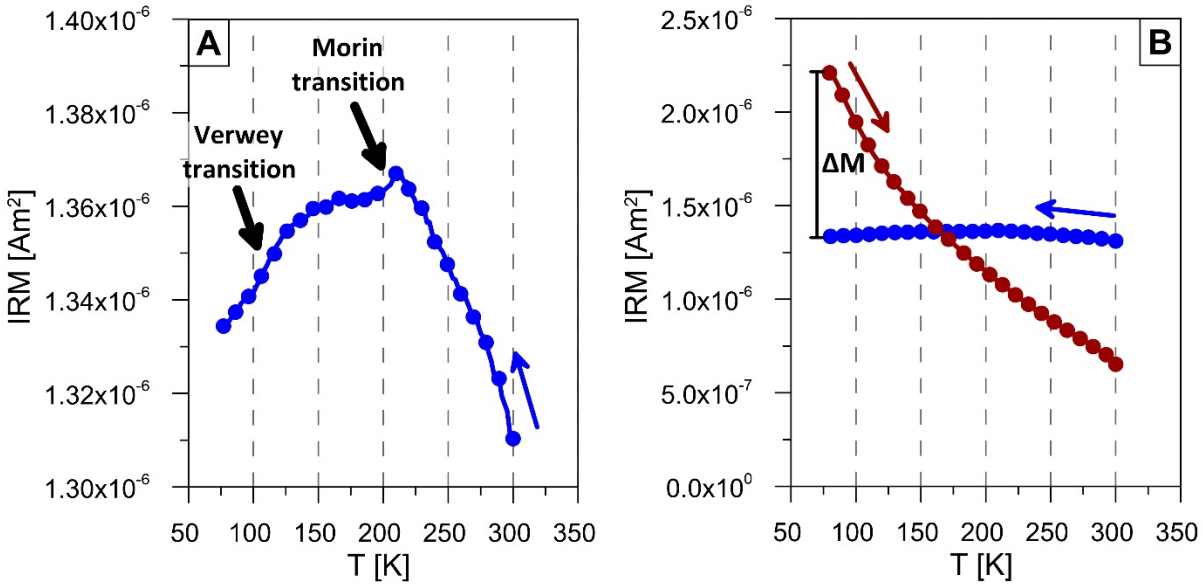

Figure 3. Low-temperature measurements for stage 11 (~2.5 µm) brake-wear emissions: (A) zero-field changes in IRM during cooling, after acquisition of IRM (at 5T) at room temperature; and (B) the same cooling changes (blue curve) and zero-field changes of IRM while heating after acquisition of IRM (at 5T) at 77K (red curve). ΔM reflects the contribution of superparamagnetic grains.

Scanning (SEM) and transmission (TEM) electron microscopy

Two brake-wear samples (stage 10 with particle size of ~1.6 µm and stage 11 with particle size of ~2.5 µm) were analysed using SEM and TEM. Figure 4 shows an overview SEM image of brake-wear particulate emissions (stage 11, ~2.5 µm). The sample is dominated by agglomerates of UFPs (one of which is marked '1'), with smaller numbers of larger grains with smooth surfaces and sharp edges (marked '2'). The larger, sharp-edged particles were also observed in our previous study (Kukutschová *et al*., 2011). The size of the UFP agglomerates and the smooth, larger grains ranges between ~0.8 µm and 9 µm. Both agglomerates and larger grains have similar elemental composition, typical of brake emissions, with Fe, C and O being dominant, and with smaller amounts of Cu, Al, Si, S, Sn, Mg, P and Cr (EDS spectra in Fig. 4).

Sb has sometimes been reported in brake-wear emissions and even suggested as a brake-wear tracer (e.g. Sternbeck *et al*., 2002; Bukowiecki *et al*., 2009b). In our brake-wear PM, we did not detect Sb (unsurprisingly, given its trace concentrations in the commercial brake pad used here, see Fig. SI 2.1).

The TEM images show that the agglomerates comprise prolific numbers of UFPs ~10 nm – 50 nm in size (Fig. 5, 6; see also SI 6). Elemental analysis using EDS in STEM mode showed the presence of C,

O and Fe, with variable but typically lower concentrations of various other elements, including Mg, Al, Si, S, Ti, Cr, Cu, Zn and Sn (Fig. 5). The distributions of these minor elements are not uniform over entire agglomerates; for example, Ti, Cr and Cu occur in specific nanoparticles within the agglomerate shown in Fig. 5C. In terms of mineralogy, the agglomerates are dominantly composed of magnetite (Fig. 5A, 6) and haematite (Fig. 6A), often covered with a thin shell composed of layers of graphitic/amorphous carbon (Fig. 6A). Although it is challenging to quantify the concentration of haematite using TEM, it appears to be present in lower concentration than magnetite.

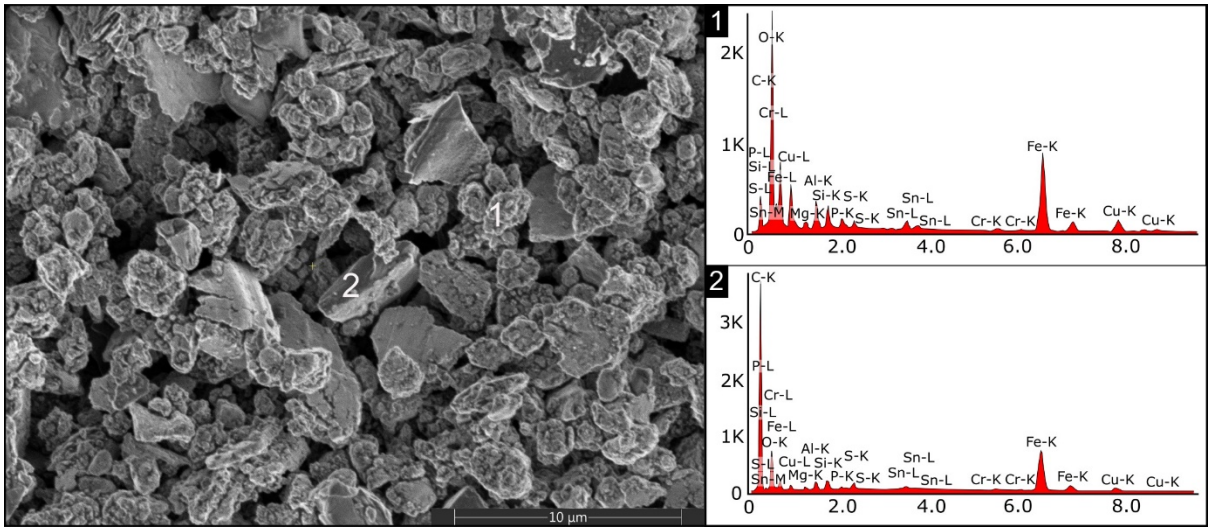

Figure 4. An overview SEM image of the stage 11 (~2.5 µm) size fraction of brake-wear emissions; EDS spectra for (1) an UFP agglomerate and (2) a large grain with smooth surface and sharp edges.

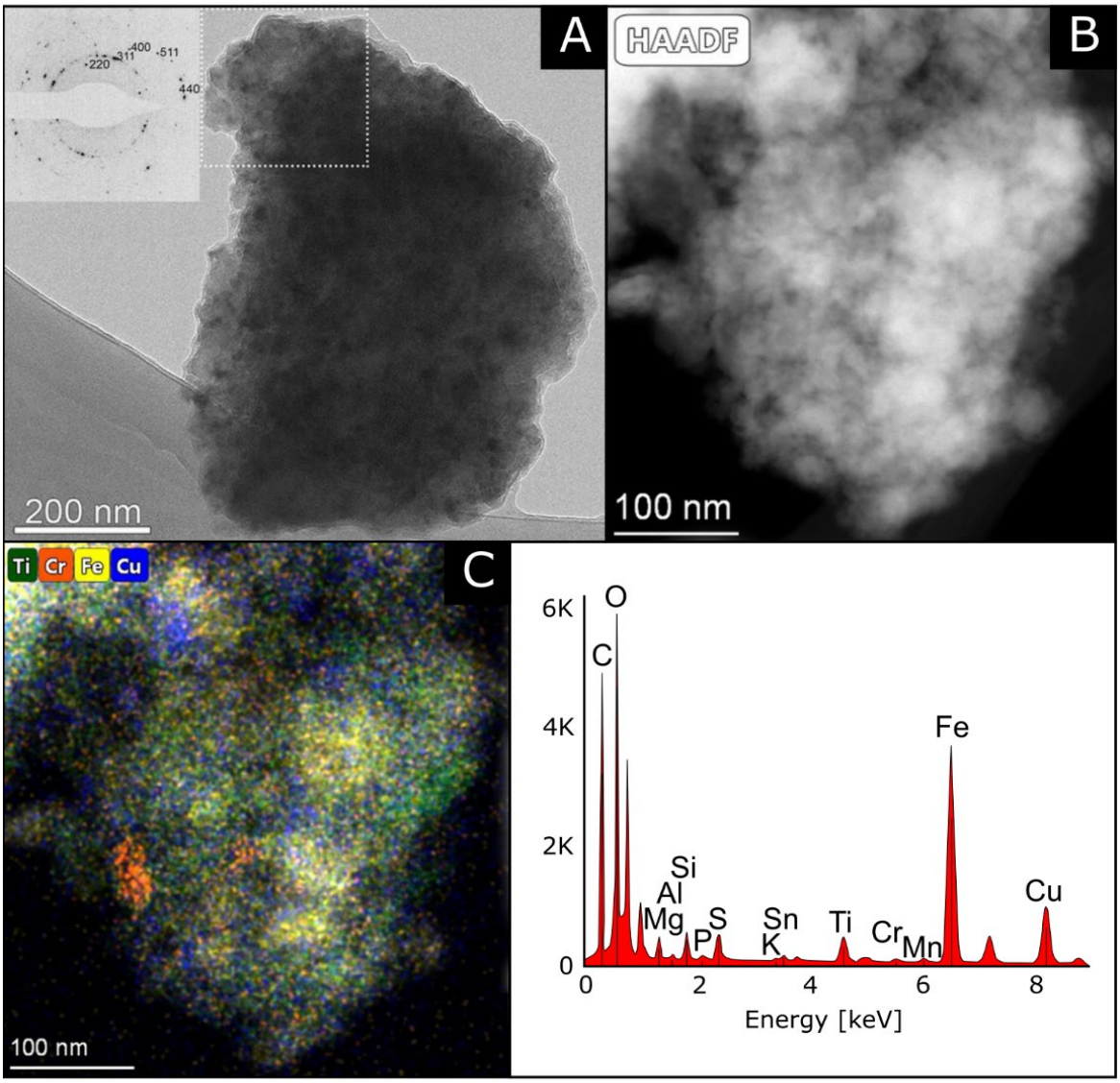

277 **Figure 5.** (A) TEM image of an UFP agglomerate with associated selected-area electron diffraction
278 pattern corresponding to an ensemble of randomly oriented magnetite nanocrystals; (B) high-angle
279 annular dark-field (HAADF) image of an UFP agglomerate found in the sample of stage 10 (~1.6 μm)
280 and (C) its EDS elemental map obtained in scanning transmission mode (STEM), showing the
281 distributions of Cr, Fe, Cu and Ti, and EDS spectra showing elemental composition.

282

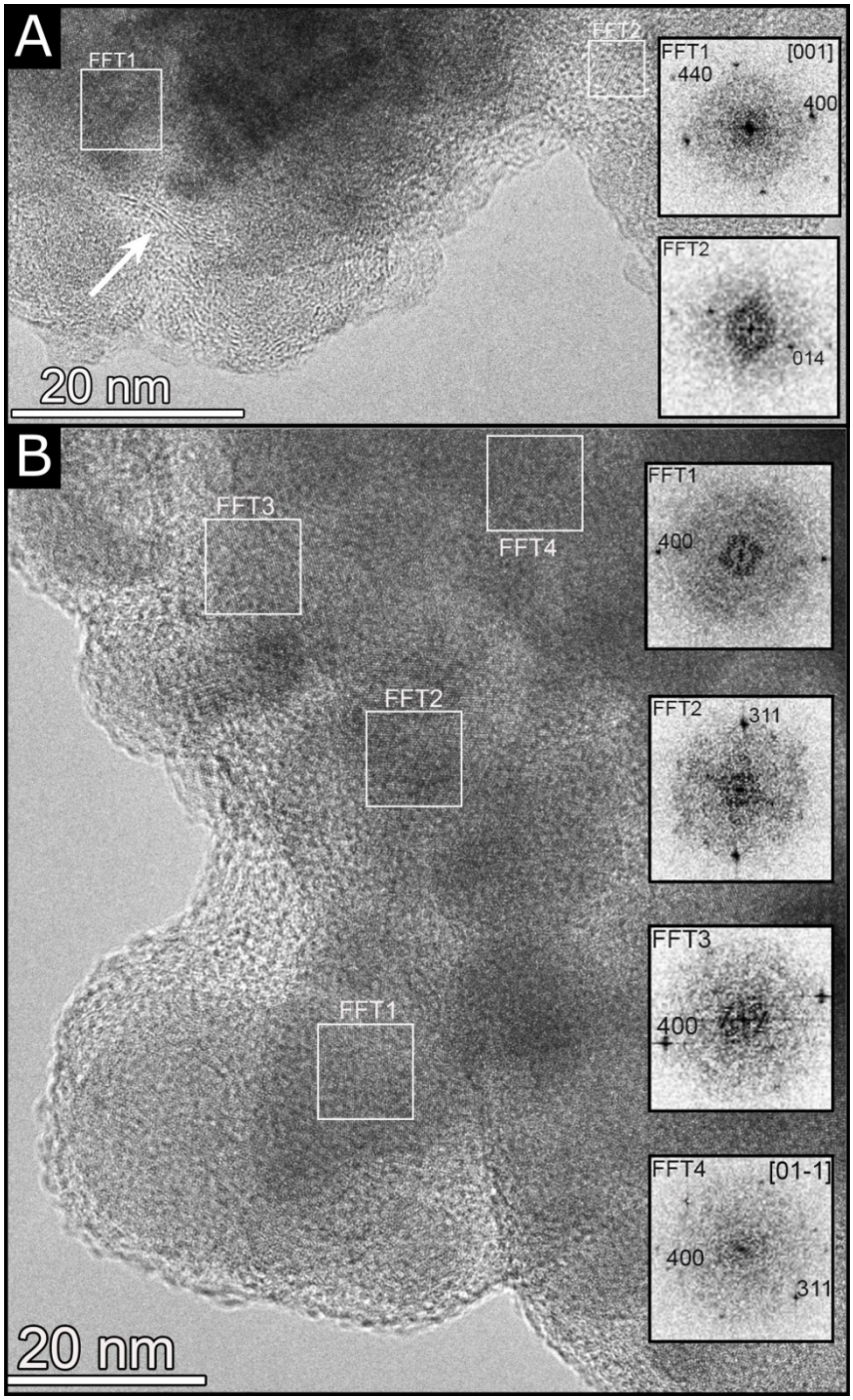

284 **Figure 6.** Structural analysis of iron oxide nanoparticles using TEM. (A) high-resolution (HRTEM) image
285 of an UFP agglomerate found in the stage 11 (~2.5 µm) sample, with associated fast Fourier
286 transforms (FFTs) of the indicated particle regions, containing reflections corresponding to
287 periodicities in magnetite (FFT1) and haematite (FFT2); the arrow marks several layers of
288 graphite/amorphous carbon with periodicity of 3.6 Å, similar to typical periodicities observed in
289 atmospheric soot; (B) HRTEM image of an UFP agglomerate with associated FFTs obtained from
290 specific particle regions, showing reflections consistent with lattice spacings in magnetite (stage 10,
291 ~1.6 µm).

Discussion

Our results show that the concentrations of Fe-rich magnetic grains in airborne brake-wear emissions are very high (~100 – 10000 times higher; cf. Fig. 1B), compared to other types of particulate pollutants produced in most urban environments (Fig. 2). Chronic exposure at the roadside or in-cabin to such high magnetite concentrations is especially worrisome because of the association of Fe-bearing (and especially magnetite) UFPs with the excess production of reactive oxygen species (ROS) in the brain, neurodegeneration and Alzheimer's disease (e.g., Plascencia-Villa *et al*., 2016; Coccini *et al.,* 2017; Maher, 2019). In addition to roadside environments with frequent braking (e.g. close to traffic-control lights or speed bumps), Fe-rich UFPs occur in high concentrations in other environments, including underground subway/train stations (Moreno *et al*., 2015) and areas affected by airborne emissions from iron-/steelworks (Li *et al*., 2021).

The oxidation state of Fe in airborne PM appears important in terms of its health hazard (e.g., Smith *et al*., 1997; Maher, 2019). Surface coatings (e.g. graphite/amorphous carbon; Fig. 6A) of UFPs might also change the uptake, distribution, clearance and toxicity of Fe-rich UFPs (e.g. Singh *et al*., 2010; Feng *et al*., 2018). Most brake-wear studies, however, have so far focused on mass and/or number concentrations of brake-wear emissions (e.g. Perricone *et al*., 2017; Alemani *et al*., 2018; Matějka *et al*., 2020); few have analysed the elemental composition of the emitted particles (e.g. Menapace *et al*., 2020), and almost none have studied the phase composition of the released particles. Given that magnetite contains Fe^{2+}, reportedly toxic to human cells through its catalysis of the Fenton reaction (e.g. Smith *et al*., 1997), and that UFPs constitute the majority of brake-wear particles (both as discrete particles (collected by ultrafine size fractions of the impactor; Fig. 1A) and agglomerates (collected by larger size fractions of the impactor; Figs. 4 – 6)), a thorough, size-resolved evaluation of elemental, mineralogical and structural composition of airborne brake-wear emissions may be critical for further assessment of potential health impact.

Several different magnetic phases have been reported previously in brake emissions: haematite, magnetite, maghemite, wüstite and metallic Fe (e.g., Kukutschová & Filip, 2018). Here, we identified 3 magnetic components in brake emissions (cf. SI 2). No component can correspond to wüstite as its Neél temperature is 200 – 210 K (Cornell & Schwertman, 2003) so it does not carry magnetic remanence at room temperature (~290 K). Moreover, the Neél temperature of wüstite was not observed on the heating curve from 77 K to room temperature (Fig. 3B), excluding its presence in our analysed brake-wear samples.

The magnetic 'hardness' (high MDF_{IRM} of 81 mT) of component C2 suggests that it represents haematite. Haematite has previously been observed in other brake-wear studies (using Raman microspectroscopy, TEM/EDS and XRD) (review in Kukutschová & Filip, 2018). The presence of haematite in our dynamometer-generated brake-wear samples from low-metallic brake pads is evident from the Morin transition in the cooling curves (Fig. 3A). Based on MDF_{IRM} data for synthetic haematite and our measured MDF_{IRM} of ~81 mT, C2 corresponds to haematite grains of ~120 nm in diameter (cf. SI 2). Based on IRM data for pure, synthetic haematite powders (see SI 2; Maher *et al*., 2004), it is possible to estimate mass concentrations (wt.%) of this mineral in the analysed samples. Hence, we estimate the average haematite mass concentration to be ~54.6 wt.% in the PM_{10} of airborne brake-wear emissions. However, due to haematite's low IRM (~25 – 60 times lower than that of magnetite, and ~450 times lower than of metallic Fe; cf. Table SI 2.2) and very low contribution to total IRM (~5.6%; Table SI 2.1), the inherent uncertainty of this estimated haematite mass concentration is very high, reaching levels up to ±32.8 wt.% (see SI 4 for more details). Although haematite was observed in TEM analysis (Fig. 6A), its concentration appears much less than the 50 wt.% estimated using magnetic component analysis. It is, therefore, highly likely that the haematite mass concentration is magnetically over-estimated here.

Since the Verwey transition was observed in the cooling curve (Fig. 3A), at least one of the 'soft' magnetic components (with relatively low MDF_{IRM} of 12 mT (C1) or 28 mT (C3)) comprises magnetite. Component C3 probably represents magnetite due to its higher MDF_{IRM} (28 mT for C3 vs 12 mT for C1; Table SI 2.1). Based on magnetic contributions from magnetic component analysis and average IRMs for sized magnetite particles (Maher, 1988), we can estimate the mass concentration of magnetite (see SI 2 for details on the estimation method). On average, the mass concentration of magnetite is ~20.2 wt.% of the total PM_{10} of brake emissions (~18.5 wt.% in $PM_{2.5}$ and ~7.6 wt.% in $PM_{0.2}$) (see SI 4 for details on the error estimations). It is likely that component C3 reflects a partially oxidised (maghemitised) magnetite, with a high contribution of SP grains, as indicated by the low-temperature magnetic properties (Fig. 3). Magnetite has been observed, but not quantified, previously in brake-wear emissions (from low-metallic brake pad/cast iron disc) (Kukutschová et al., 2010, 2011; Peikertová et al., 2013; Verma et al., 2016; Kukutschová & Filip, 2018).

The remaining component, C1, probably corresponds to metallic Fe, as indicated by high-temperature changes in magnetic susceptibility (SI 3). Its concentration is ~1.6 wt.% (see also SI 4 for the estimation uncertainties and SI 2 for details on the estimation method).

The mass concentrations of all three magnetic phases generally decline with decreasing particle size (Figure SI 2.4). Magnetite concentrations reach levels ~20 wt.% for particles > 0.600 µm and

decrease to 2 – 15 wt.% for particles < 0.380 µm. Metallic Fe content ranges between ~2.0 wt.% for size fractions > 1.6 µm and < 0.5 wt.% for particles < 0.400 µm. The physical and chemical processes occurring within brake systems while braking are complex, abrupt and irregular (e.g. Kukutschová *et al*., 2009; Lee & Filip, 2013; Nosko *et al*., 2015; Kukutschová & Filip, 2018). Magnetic particles can be released from the magnetite filler that is often added to brake pads as solid lubricant, Fe/steel fibres used as reinforcing constituents (Jang, 2013; Kukutschová & Filip, 2018), and/or the cast iron brake disc. The XRD spectrum for the brake pad used in this study showed the presence of various phases of Fe, including metallic Fe (α-Fe), Fe oxides (magnetite/maghemite) and Fe oxide-hydroxides (Fig. SI 2.1). The 3-component magnetic composition of Fe-bearing particles we identify in our brake-wear emissions may reflect either or both the release of abraded particles from the brake pad and friction-derived modification of particles through increasing stages of oxidation, from metallic Fe (in both brake pad and disc), through magnetite (potentially partially oxidised/mixed with maghemite), and finally to haematite.

Although brake systems are designed to abrade friction materials of brake pads and discs, our data show that high-temperature oxidation, evaporation and condensation processes are also important, creating very high numbers of discrete, rounded/spherical UFPs, which can subsequently be released to the atmosphere both as discrete UFPs (> 99% of PNC; Fig. 1) and as agglomerates of UFPs (dominating larger size fractions; Figs. 4 – 6). Interestingly, some authors have observed PM emissions (both solid and semi-volatile) from braking systems even without applying brakes, presumably due to similar evaporation/condensation processes (Wahlström & Olofsson, 2014; Hagino *et al.*, 2015, 2016; Ma *et al*., 2020). These processes depend on the friction materials, braking conditions (e.g. braking frequency, applied pressure, air humidity), and even the age of the friction materials (due to rust). In general, below ~200^{0}C, the abrasive processes usually dominate and larger (> 1 µm) wear particles are mostly emitted. At higher temperatures (> 160^{0}C – 190^{0}C), the concentration of UFPs (< 0.1 µm) increases considerably due to high-temperature oxidation, evaporation and condensation processes (e.g. Garg *et al*., 2000, Kukutschová *et al*., 2010, 2011; Verma *et al*., 2016; Piscitello *et al*., 2021). These ultrafine particles subsequently agglomerate and form larger aggregates, such as these observed in our SEM/TEM images (Figs. 4 – 6 and SI 6). Importantly, only impactors/particle sizers (e.g. ELPI+, OPS and/or SMPS) are conventionally used to evaluate particle size distributions of brake-wear emissions. Without further analysis (e.g. using SEM and/or TEM), it is impossible to distinguish between discrete larger grains and agglomerates of UFPs, since both of these are classified as 'large' particles by an impactor/particle sizer. Hence, in many studies the presence of agglomerated ultrafine particles in coarse fractions is not analysed or discussed whatsoever.

The magnetic properties of brake-wear emissions deposited on vehicle wheel rims have been investigated in several studies (Sagnotti *et al*., 2009; Chaparro *et al*., 2010; Marié *et al*., 2010; Sagnotti & Winkler, 2012). Chaparro *et al*. (2010), for example, observed IRM of these wheel deposits to be between $569.6 \cdot 10^{-3}$ Am^2/kg and $1201 \cdot 10^{-3}$ Am^2/kg, substantially lower than the IRMs of the non-airborne brake wear we obtained here ($\sim 8891 \cdot 10^{-3}$ Am^2/kg). These previous studies suggested that brake-wear PM is dominated by magnetic grains > 0.1 μm or even > 1 μm (albeit with uncertainty regarding any SP fraction) (Sagnotti *et al*., 2009; Chaparro *et al*., 2010; Marié *et al*., 2010; Sagnotti & Winkler, 2012). However, our results, based on size-fractionated airborne brake emissions, show high IRMs for all collected size fractions, including those smaller than 0.1 μm (Fig. 2). This discrepancy probably reflects different methods of sample collection. Here, we collected particles which had originated from the friction couple (brake pad/cast iron disc), during braking, using a full-scale dynamometer and one formulation of brake pads; and analysed the magnetic properties of this size-fractionated brake-wear. Most UFPs emitted from car braking systems probably do not settle on the wheel rim, but are released to the roadside air. It is also likely that PM samples settled on wheel rims, contain, besides highly magnetic brake wear particles, some portion of tyre wear, roadside and soil-derived re-suspended PM, which display lower IRMs (cf. Fig. 1B and Gonet *et al*., 2021). Thus, the wheel-deposited PM mixture has lower magnetic content than our 'pure' brake wear particles. The age of brake pads might also be important. In the dynamometer experiments, we used a new set of brake pads and discs, whereas car brake pads often rust as they age. As rust is a mixture of hydrous Fe oxides and Fe oxide-hydroxides (rather than 'pure', well-crystalline Fe oxides, e.g. highly magnetic magnetite), the measured IRM of such 'aged' brake emissions will be lower compared to 'new' friction materials from dynamometer experiments. Vehicle-derived rust might contribute to the ferrihydrite reported by Pattammattel *et al*. (2021) in roadside PM analysed in Los Angeles, USA. Moreover, wheel rim-deposited PM might oxidise with residence time in the urban air (metallic Fe oxidising to magnetite/maghemite, and then into haematite). Each oxidation stage will decrease the final, measured IRM value of such deposited material.

Various studies show the abundant presence of Fe-bearing UFPs in roadside PM (e.g. Ntziachristos *et al.*, 2007; Sanderson et al., 2014, 2016; Yang *et al*., 2016; Gonet & Maher, 2019; Long *et al*., 2020; Zhang *et al*., 2020). Magnetic data for roadside PM have also shown the presence of ultrafine, SP grains (< ~30 nm) in roadside air pollution (e.g., Muxworthy *et al.*, 2002, 2003; Sagnotti *et al.*, 2006, 2009). However, SP grains could occur as discrete ultrafine grains and/or as oxidized rims around larger particles, arising from cracking of cation-deficient coatings of the unoxidised core (Özdemir *et al*., 1993; Muxworthy *et al*., 2002, 2003; Sagnotti *et al*., 2009, Sagnotti & Winkler, 2012; Rea-Downing *et al*., 2020). Indeed, specifically for particulate brake-wear emissions, magnetic studies have provided

contradictory data on the presence of discrete ultrafine SP grains versus SP oxidised rims around larger magnetic grains (Sagnotti *et al*., 2009; Sagnotti & Winkler, 2012). Our low temperature (77 K) magnetic measurements identify that the SP contribution to total magnetic remanence of brake emissions varies from ~25% to 45%. In contrast, Marié *et al*. (2010) obtained very low values (0.0 – 0.8%) of frequency dependence of magnetic susceptibility ($\kappa_{fd\%}$) for brake wear. This parameter is sensitive to the presence of SP grains and is usually higher than ~5% - 6% in the presence of SP grains (Dearing *et al*., 1996). Here, we also obtained low $\kappa_{fd\%}$, ranging between 0.5% and 3.4% (data not shown). To resolve these apparently contradictory magnetic data, we used, besides low-temperature magnetic measurements, an independent analytical approach, TEM.

Our TEM analysis shows that agglomerated UFPs dominate even the larger size fractions (~1.6 µm – 2.5 µm) of brake-wear emissions, consistent with our previous study (Kukutschová *et al.*, 2011). These aggregates comprise rounded/spherical particles ~10 nm – 50 nm in size, abundant in Fe oxides, with smaller concentrations of Al, Cu, Si, Sn, Mg, Cr, Mn and Zn, in places surrounded by or embedded in C (see SI 6). The presence of C is probably a product of the oxidative wear of phenolic resin, used in brake pads as a binder (Filip *et al*., 2002; Kukutschová & Filip, 2018). Liati *et al*. (2019) found brake-derived agglomerates of UFPs, with similar rounded/spherical morphology and elemental composition to our agglomerates (Figs. 4 – 6; SI 6). We did not observe SP oxidised rims using TEM, and the presence of such prolific numbers of agglomerated, magnetic UFPs can readily account for the observed SP behaviour, i.e., the large increase in IRM at 77K (Fig. 3B).

Interestingly, we observed measurable magnetic remanence for all size fractions, including those smaller than 30 nm (stages 1 and 2 in Fig. 2). Theoretically, magnetite grains < 30 nm, haematite < 27 nm and metallic Fe < 8 nm should not hold any magnetic remanence at room temperature due to thermal agitation of their moments, hence resulting in SP behaviour (Dunlop, 1973; Özdemir *et al*., 1993; Bødker & Mørup, 2000; Pankhurst *et al*., 2008). Magnetic component analysis suggests that metallic Fe is responsible for only ~36% of IRM for stages 1 and 2 (< 30 nm; Fig. SI 2.2); hence, the measurable IRM of these ultrafine particle size fractions likely reflects magnetic interactions of SP grains of magnetite, resulting in collective SD-like behaviour. Similar effects were observed by Radhakrishnamurty *et al*. (1973) and Maher (1988). This collective, SD-like behaviour might also explain the low values of frequency dependent magnetic susceptibility for brake-wear emissions obtained in our study, and by Marié *et al*. (2010).

The very strongly magnetic nature of brake-derived PM also has important consequences for interpreting magnetic monitoring studies, regarding the properties and sources of the magnetic PM deposited on biological surfaces (e.g., see review by Hofman *et al*., 2017). Sagnotti *et al*. (2009) and

Sagnotti & Winkler (2012) compared the magnetic properties of roadside PM, petrol, diesel, and brake emissions. They noted close resemblance between the magnetic properties of brake emissions and the roadside PM accumulated on air filters and roadside leaves. This now appears unsurprising, given that brake-derived magnetite might constitute 68% – 85% of total airborne magnetite in the roadside environment, as estimated in our recent study (Gonet *et al*., 2021). Moreover, the presence of brake-derived metallic Fe might be another confounding factor.

Air pollution in urban environments occurs in spatially and temporally variable concentrations, changing from country to country, town to town, even from one side of the street to another (Matzka & Maher, 1999). Locally, air pollution levels depend on the proximity to major roads, traffic characteristics, local road structure and topography, time of the day, weather conditions and season (e.g. Jeong et al., 2015; Pasquier & André, 2017). Specifically, high concentrations of brake-wear emissions are expected in proximity to traffic-control lights (or speed bumps), or where traffic jams are frequent, and braking (and accelerating) is repetitive. At such sites, co-association between brake-derived PM and engine exhaust emissions might explain the correlation between concentration-dependent magnetic parameters (e.g. IRM) and exhaust-related metals (e.g. Pb) (Maher *et al*., 2008), even though the magnetic properties of roadside PM might be dominated by brake-wear emissions, rather than by engine-exhaust PM (Gonet *et al*., 2021). However, at other heavily polluted urban sites (e.g. close to highways where engine exhaust emissions dominate), brake-derived PM is likely to occur in low (or sometimes negligible) concentrations due to rather sporadic braking.

Indeed, this inter-correlation between the concentrations of different traffic-related sources of PM in some sites (e.g. close to traffic lights) and lack of such correlation at other sites (e.g. close to freeways) might be a key reason why source apportionment of different traffic-derived sources of PM in urban environments is challenging and variable between different studies and sampling sites (e.g. Bukowiecki *et al*., 2009a; Harrison *et al*., 2011, 2012; Lawrence *et al*., 2013). Thus, careful selection of different types of roadside sampling sites is essential for characterising and quantifying different roadside PM sources, and resultant human exposure levels to those different sources.

Notably, over 99% of the PNC of our solid (non-volatile) brake-wear particles is smaller than ~200 nm (Fig. 1). Moreover, even larger particle collection stages are dominated by agglomerates of UFPs ~10 nm – 50 nm in diameter (Figs. 4 – 6), which, depending on particle/cell interactions, have the potential to release millions of discrete UFPs inside the human body. Such small particles have been shown to reach almost all major organs, including the brain; the latter accessible directly by inhalation via the olfactory bulb (Oberdörster *et al*., 2004; Maher *et al.*, 2016), and/or indirectly through ingestion/swallowing and transfer via the gut wall and neuroenteric system (Calderón-Garcidueñas *et*

490 *al.,* 2020), and/or via the systemic circulation. The presence of magnetite, Fe- and other metal-rich air
491 pollution UFPs has been demonstrated recently in the blood serum, and pleural effusions, of residents
492 living in Beijing, China (Lu *et al*., 2020).

493 Maher *et al*. (2016) and Calderón-Garcidueñas *et al*. (2020) observed exogenous,
494 rounded/spherical UFPs (usually < 150 nm) of Fe-rich composition, including magnetite, in frontal
495 cortex and brainstem tissues, similar to those found in the brake emissions in this (Fig. 5, 6) and
496 previous studies (Kukutschová *et al*., 2010). Exogenous, carbon- and Fe-rich UFPs have also been found
497 in other human tissues, including heart (Calderón-Garcidueñas *et al*., 2019b; Maher *et al*., 2020),
498 human serum and pleural effusions (Lu *et al.,* 2020), placenta (Bové *et al*., 2019; Liu *et al*., 2021) and
499 amniotic fluid (Barošová *et al.*, 2015). These UFPs are usually associated both with other metals (e.g.,
500 Al, Ca, Ce, Co, Cr, Cu, Mn, Ni, Pt, Ti, Sn and Zn) (Barošová *et al.*, 2015; Maher *et al*., 2016; Bové *et al*.,
501 2019; Calderón-Garcidueñas *et al*., 2019b, 2020; Lu *et al*., 2020; Liu *et al*., 2021) and with evidence of
502 biological dysfunction, e.g. misfolded proteins, neurites and mitochondrial damage in the brainstem
503 (Calderón-Garcidueñas *et al*., 2020), and mitochondrial damage and ventricular up-regulation in the
504 heart (Calderón-Garcidueñas *et al*., 2019b; Maher et al., 2020).

505 In the roadside environment, various toxic metals (e.g. Al, Ba, Cu, Fe or Mn) (Gao *et al*., 2020), and
506 especially potentially neurotoxic magnetite, originate abundantly from brake wear (Thorpe &
507 Harrison, 2008; Kukutschová *et al*., 2010, 2011; Peíkertová *et al*., 2013; Straffelini *et al*., 2015;
508 Peíkertová & Filip, 2016; Verma *et al.*, 2016; Kukutschová & Filip, 2018; Gonet *et al*., 2021). Both Fe
509 and Cu might catalyse ROS production (Smith *et al*., 1997; Allsop *et al*., 2008; Charrier & Anastasio,
510 2011; Tabner *et al*., 2010; Li & Reichmann, 2016; Gao et al., 2020). Further, mixtures of metals (e.g. Fe
511 and Cu) can act synergistically to promote oxidative cell damage (Charrier & Anastasio, 2011).
512 Exposure to Ba, found in human amniotic fluid (Barošová *et al.*, 2015), might additionally lead to
513 cardiovascular, renal, metabolic, neurological and mental disorders (e.g. Kravchenko *et al*., 2014).
514 Hence, brake-wear particulate emissions, rich in potentially toxic metals and organic matter, might
515 exert adverse impacts on various human organs, including the brain, at every life stage, from foetal to
516 adult.

517 *In vitro* and *in vivo* studies of the pulmonary and cardiovascular toxicity of brake wear PM (both
518 'airborne' and 'non-airborne' fractions) show that brake emissions can cause oxidative stress and
519 chromosomal damage, invoke pro-inflammatory responses and increase ROS production (Gasser *et*
520 *al*., 2009; Kukutschová *et al*., 2009; Zhao *et al*., 2015; Kazimirova *et al*., 2016; Malachova *et al*., 2016;
521 Barosova *et al*., 2018; Puisney *et al*., 2018; Rajhelová *et al*., 2019; Selley *et al*., 2019). Given the
522 predominance of UFPs (99% of PNC < 200 nm; Fig. 1) in brake-wear emissions, our identification of

high concentrations of magnetite in $PM_{0.2}$ (~7.6 wt.%) and its reported association with neurodegenerative diseases, it seems both timely and important for the neurotoxic potential of the specific components of brake-wear emissions to be investigated in detail. Indeed, the impacts of Fe and other transition metals in airborne PM are likely under-estimated in such studies at present, due to assay-induced metal precipitation/immobilization, e.g. in phosphate-buffered systems (Reed *et al*., 2021).

The ISO26867 dynamometer cycle, used in this study, is an established and commonly used brake dynamometer cycle in mechanical and tribological studies of brake systems. It covers a wide variety of driving and braking conditions, including, among others, harsh braking events which likely happen only episodically in urban areas. This cycle might thus not be fully representative for urban driving. Brake pad/disc temperature is a critical parameter in terms of the release of ultrafine particles. During the ISO26867 cycle, this temperature can reach levels higher than these usually occurring when driving in cities (e.g. Nosko et al., 2015, 2017; Perricone et al., 2017; Alemani et al., 2018). Follow-up magnetic, elemental and morphological analyses of brake-wear emissions, using a less severe brake cycle (e.g. the WLTP-based cycle proposed by Mathissen et al., 2018) would be valuable for further characterising and understanding the generation and concentration of brake-derived UFPs.

In this study, we tested and analysed PM emissions from an example of a brake system for a middle-size passenger car, commercially-available and widely-used on the European market. Although the range of friction materials used on the global market is very wide (e.g. Hulskotte *et al.,* 2014), our magnetic and compositional data are generally in line with other studies of brake-wear emissions. The three magnetic phases observed in this study (i.e. magnetite, haematite and metallic Fe) have been reported (but not quantified) by other authors (e.g. Peikertová *et al.,* 2013; Verma *et al.,* 2016; Kukutschová & Filip, 2018). Our SEM/TEM analyses showed the presence of Fe, C and O, with lower concentrations of Cu, Al, Si, S, Sn, Mg, P and Cr (cf. Figs. 4 and 5). All these elements have been commonly observed in brake-wear emissions (e.g. review in Kukutschová & Filip, 2018). Hence, our results seem to be representative for commonly used friction materials.

Conclusions

Combining magnetic component analysis (based on magnetic remanence), low-temperature and high-field magnetic measurements, and electron microscopy enabled, for the first time, size-resolved quantitative evaluation of the magnetic mineralogy of airborne brake-wear emissions.

We observed three magnetic phases: haematite; magnetite; and metallic Fe. From the magnetic component analysis, the average magnetite concentration in total PM_{10} of brake emissions is ~20.2 wt.%, metallic Fe ~1.6 wt.%, and haematite ~54.6 wt.%. The haematite concentration is likely magnetically over-estimated (high uncertainty being associated with its much lower IRM compared with magnetite and metallic Fe).

Most brake-wear particles (> 99% of PNC) are smaller than 200 nm. Brake-wear emissions exhibit a strong superparamagnetic signal, reflecting the presence of very high numbers of UFPs < ~30 nm in size. Even the larger brake-wear PM size fractions are dominated by agglomerates of ultrafine, superparamagnetic grains, which explains their low-temperature increase in IRM. Depending on interactions between these agglomerates and potential biological targets, release of discrete UFPs might result in chronic supply of toxic metal-bearing UFPs to all major organs of the body. Such UFPs likely pose a threat to neuronal and cardiovascular health after inhalation and/or ingestion. The concentration of magnetite in brake-wear particle sizes smaller than 200 nm ($PM_{0.2}$) is estimated to be ~7.6 wt.%. Magnetite particles < 200 nm might be especially hazardous to the brain and the heart, contributing both to microglial inflammatory action, and catalysis of the Fenton reaction, leading to excess ROS production, and cell damage due to oxidative stress.

Given this predominance of UFPs in non-volatile brake-wear emissions, high concentrations of magnetite in $PM_{0.2}$, and the reported association between excess Fe and neurodegenerative diseases, the neurotoxic potential of brake-wear emissions warrants detailed investigation. We hypothesise that chronic exposure to such particles can plausibly account for the observed PM dose/response relationships reported for cardiovascular disease, and for neurodegenerative diseases, including Alzheimer's and Parkinson's disease.

Finally, based on current knowledge, it is evident that particulate emissions generated by wear of brake pads/discs can be controlled by modification of brake pad formulation and/or brake pads/disc coatings. However, great care is required in order to avoid the risk of exchanging one health hazard (e.g. asbestos used in brake formulations before ~1990) for another (e.g. cytotoxic metal-rich UFPs). Another potentially effective strategy to limit brake emissions is the replacement of standard, friction brakes by regenerative brake systems, increasingly implemented by manufacturers of electric vehicles.

ACKNOWLEDGEMENTS

T. Gonet is funded by a PhD studentship from Jaguar Land Rover. We thank Dr. Vassil Karloukovski, Dr. James Cumby, and Kateřina Mamulová-Kutláková for their help with laboratory work. We are also grateful to Dr. Ramon Egli who kindly provided us with CODICA and GECA software. The authors also thank the support of the project LTI19008 – National Contact Centre for Non-Exhaust Emissions from Traffic funded by Ministry of Education, Youth and Sports of the Czech Republic. Nanolab at the University of Pannonia received funding from the National Research, Development and Innovation Fund of Hungary under grant numbers GINOP-2.3.2-15-2016-00017, GINOP-2.3.3-15-2016-0009 and TKP2020-IKA-07. We appreciate the thoughtful comments provided by the reviewers.

REFERENCES

1. Adachi, K.; Tainosho, Y. Characterization of heavy metal particles embedded in tire dust. *Environment International* **2004**, 30, 1009-1017.
2. Alemani, M.; Wahlström, J.; Olofsson, U. On the influence of car brake system parameters on particulate matter emissions. *Wear* **2018**, 396-397, 67-74.
3. Allsop, D.; Mayes, J.; Moore, S.; Masad, A.; Tabner, B. J. Metal-dependent generation of reactive oxygen species from amyloid proteins implicated in neurodegenerative disease. *Biochemical Society Transactions* **2008**, 36, 1293-1298.
4. Barosova, H.; Chortarea, S.; Peikertova, P.; Clift, M. J. D.; Petri-Fink, A.; Kukutschova, J.; Rothen-Rutishauser, B. Biological response of an in vitro human 3D lung cell model exposed to brake wear debris varies based on brake pad formulation. *Archives of Toxicology* **2018**, 92, 2339-2351.
5. Barošová, H.; Dvořáčková, J.; Motyka, O.; Kutláková, K. M.; Peikertová, P.; Rak, J.; Bielniková, H.; Kukutschová, J. Metal-based particles in human amniotic fluids of foetuses with normal karyotype and congenital malformation - a pilot study. *Environmental Science and Pollution Research* **2015**, 22 (10), 7582−7589.
6. Beddows, D. C. S.; Harrison, R. M.; Green, D. C.; Fuller, G. W. Receptor modelling of both particle composition and size distribution from a background site in London, UK. *Atmospheric Chemistry and Physics* **2015**, 15, 10107-10125.
7. Beelen, R.; Raaschou-Nielsen, O.; Stafoggia, M.; Jovanovic Andersen, Z.; Weinmayr, G.; Hoffmann, B.; Wolf, K.; Samoli, E.; Fischer, P.; Nieuwenhuijsen, M.; *et al*. Effects of long-term exposure to air pollution on natural-cause mortality: an analysis of 22 European cohorts within the multicentre ESCAPE project. *Lancet* **2014**, 383, 785−795.
8. Bødker, F.; Mørup, S. Size dependence of the properties of hematite nanoparticles. *Europhysics Letters* **2000**, 52(2), 217-223.
9. Bové, H.; Bongaerts, E.; Slenders, E.; Bijnens, E. M.; Saenen, N. D.; Gyselaers, W.; Van Eyken, P.; Plusquin, M.; Roeffaers, M. B. J.; Ameloot, M.; Nawrot, T. S. Ambient black carbon particles reach the fetal side of human placenta. *Nature Communications* **2019**, 10, 3866.
10. Bukowiecki, N.; Gehrig, R.; Lienemann, P.; Hill, M.; Figi, R.; Buchmann, B.; Furger, M.; Richard, A.; Mohr, C.; Weimer, S.; Prévôt, A.; Baltensperger, U. *PM10 emission factors of abrasion particles from road traffic*; TRIMIS: Schweiz, Eidgenoss, **2009a**; p. 1268.
11. Bukowiecki, N.; Lienemann, P.; Hill, M.; Figi, R.; Richard, A.; Furger, M.; Rickers, K.; Falkenberg, G.; Zhao, Y.; Cliff, S. S.; Prevot, A. S. H.; Baltensperger, U.; Buchmann, B.; Gehrig, R. Real-world emission factors for antimony and other brake wear related trace elements: Size-segregated

values for light and heavy duty vehicles. *Environmental Science & Technology* **2009b**, 43, 8072-8078.

12. Calderón-Garcidueñas, L.; Azzarelli, B.; Acuna, H.; Garcia, R.; Gambling, T. M.; Osnaya, N.; Monroy, S.; Del Rosario Tizapantzi, M.; Carson, J. L.; Villareal-Calderon, A.; Rewcastle, B. Air pollution and brain damage. *Toxicologic Pathology* **2002**, 30(3), 373-389.
13. Calderón-Garcidueñas, L.; Mukherjee, P. S.; Kulesza, R. J.; Torres-Jardón, R.; Hernández-Luna, J.; Ávila-Cervantes, R.; Macías-Escobedo, E.; González-González, O.; González-Maciel, A.; García-Hernández, K.; Hernández-Castillo, A.; Research UVM Group, Villareal-Ríos, R. Mild cognitive impairment and dementia involving multiple cognitive domains in Mexican urbanities. *Journal of Alzheimer's Disease* **2019a**, 68(3), 1113-1123.
14. Calderón-Garcidueñas, L.; González-Maciel, A.; Mukherjee, P. S.; Reynoso-Robles, R.; Pérez-Guillé, B.; Gaynosso-Chávez, C.; Torres-Jardón, R.; Cross, J. V.; Ahmed, I. A. M.; Karloukovski, V. V.; Maher, B. A. Combustion- and friction-derived magnetic air pollution nanoparticles in human hearts. *Environmental research* **2019b**, 176, 108567.
15. Calderón-Garcidueñas, L.; González-Maciel, A.; Reynoso-Robles, R.; Hammond, J.; Kulesza, R.; Lachmann, I.; Torres-Jardón, R.; Mukherjee, P. S.; Maher, B. A. Quadruple abnormal protein aggregates in brainstem pathology and exogenous metal-rich magnetic nanoparticles (and ingineered Ti-rich nanorods). The substantia nigrae is a very early target in young urbanities and the gastrointestinal tract a key brainstem portal. *Environmental Research* **2020**, 191, 110139.
16. Castellani, R. J.; Moreira, P. I.; Liu, G.; Dobson, J.; Perry, G.; Smith, M. A.; Zhu, X. Iron: The redox-active center of oxidative stress in Alzheimer disease. *Neurochemical Research* **2007**, 32, 1640-1645.
17. Chaparro, M. A. E.; Marié, D. C.; Gogorza, C. S. G.; Navas, A.; Sinito, A. M. Magnetic studies and scanning electron microscopy – X-ray energy dispersive spectroscopy analysis of road sediments, soils and vehicle-derived emissions. *Studia Geophysica et Geodaetica* **2010**, 54, 633-650.
18. Charrier, J. G.; Anastasio, C. Impacts of antioxidants on hydroxyl radical production from individual and mixed transition metals in a surrogate lung fluid. *Atmospheric Environment* **2011**, 45, 7555-7562.
19. Chen, H.; Kwong, J. C.; Copes, R.; Tu, K.; Villeneuve, P. J.; van Donkelaar, A.; Hystad, P.; Martin, R. V.; Murray, B. J.; Jessiman, B.; Wilton, A. S.; Kopp, A.; Burnett, R. T. Living near major roads and the incidence of dementia, Parkinson's disease, and multiple sclerosis: a population-based cohort study. *The Lancet* **2017**, 389(10070), 718-726.

20. Chen, J.; Zheng, H.; Wang, W.; Liu, H.; Ling, L.; Bao, L.; Ren, L. Resuspension method for road surface dust collection and aerodynamic size distribution characterization. *China Particuology* **2006**, *4*(6), 300-303.
21. Chen, J.-C.; Schwartz, J. Neurobehavioral effects of ambient air pollution on cognitive performance in US adults. *NeuroToxicology* **2009**, 30, 231-239.
22. Coccini, T.; Caloni, F.; Cando, L. J. R.; De Simone, U. Cytotoxicity and proliferative capacity impairment induced on human brain cell cultures after short- and long-term exposure to magnetite nanoparticles. *Journal of Applied Toxicology* **2017**, 37, 361-373.
23. Collingwood, J.; Dobson, J. Mapping and characterization of iron compounds in Alzheimer's tissue. *Journal of Alzheimer's Disease* **2006**, 10, 215-222.
24. Conte, M.; Contini, D. Size-resolved particle emission factors of vehicular traffic derived from urban eddy covariance measurements. *Environmental Pollution* **2019**, 251, 830-838.
25. Cornell, R. M.; Schwertmann, U. *Electronic, electric and magnetic properties and colour*. [In:] The iron oxides: Structure, Properties, Reactions, Occurrences and Uses, by Cornell, R. M.; Schwertmann, U. WILEY-VCH Verlag GmbH & Co. KGaA, **2003**, Weinheim.
26. Crilley, L. R.; Lucarelli, F.; Bloss, W. J.; Harrison, R. M.; Beddows, D. C.; Calzolai, G.; Nava, S.; Valli, G.; Bernardoni, V.; Vecchi, R. Source apportionment of fine and coarse particles at a roadside and urban background site in London during the 2012 summer ClearfLo campaign. *Environmental Pollution* **2017**, 220, 766-778.
27. Dearing, J. A.; Dann, R. J. L.; Hay, K.; Lees, J. A.; Loveland, P. J.; Maher, B. A.; O'Grady, K. Frequency-dependent susceptibility measurements of environmental materials. *Geophysical Journal International* **1996**, 124, 228-240.
28. Denier van der Gon, H.; Hulskotte, J.; Jozwicka, M.; Kranenburg, R.; Kuenen, J.; Visschedijk, A. European emission inventories and projections for road transport non-exhaust emissions. Analysis of consistency and gaps in emission inventories from EU member states. In *Non-exhaust emissions. An urban air quality problem for public health; Impact and mitigation measures*; Amato, F., Ed.; Academic Press, **2018**. https://doi.org/10.1016/B978-0-12-811770-5.00005-4
29. Donaldson, K.; Stone, V.; Clouter, A.; Renwick, L.; MacNee, W. Ultrafine particles. *Occupational and Environmental Medicine* **2001**, 58, 211-216.
30. Dunlop, D. J. Superparamagnetic and single-domain threshold sizes in magnetite. *Journal of Geophysical Research* **1973**, 78(11), 1780-1793.

31. Elder, A.; Gelein, R.; Silva, V.; Feikert, T.; Opanashuk, L.; Carter, J.; Potter, R.; Maynard, A.; Ito, Y.; Finkelstein, J.; Oberdörster, G. Translocation of inhaled ultrafine manganese oxide particles to the central nervous system. *Environmental Health Perspectives* **2006**, 114(8), 1172-1178.
32. Feng, Q.; Liu, Y.; Huang, J.; Chen, K.; Huang, J.; Xiao, K. Uptake, distribution, clearance, and toxicity of iron oxide nanoparticles with different sizes and coatings. *Scientific Reports* **2018**, 8, 2082.
33. Gao, D.; Ripley, S.; Weichenthal, S.; Pollitt, K. J. G. Ambient particulate matter oxidative potential: Chemical determinants, associated health effects, and strategies for risk assessment. *Free Radical Biology and Medicine* **2020**, 151, 7-25.
34. Garg, B. D.; Cadle, S. H.; Mulawa, P. A.; Groblicki, P. J.; Laroo, C.; Parr, G. A. Brake wear particulate matter emissions. *Environmental Science & Technology* **2000**, 34(21), 4463-4469.
35. Gasser, M.; Riediker, M.; Mueller, L.; Perrenoud, A.; Blank, F.; Gehr, P.; Rothen-Rutishauser, B. Toxic effects of brake wear particles on epithelial lung cells *in vitro*. *Particle and Fibre Toxicology* **2009**, 6(30).
36. Geiser, M.; Kreyling, W. G. Deposition and biokinetics of inhaled nanoparticles. *Particle and Fibre Toxicology* **2010**, 7(2).
37. Gonet, T.; Maher, B. A. Airborne, Vehicle-derived Fe-bearing nanoparticles in the urban environment: A review. *Environmental Science & Technology* **2019**, 53, 9970-9991.
38. Gonet, T.; Maher, B. A.; Kukutschová, J. Source apportionment of magnetite particles in roadside airborne particulate matter. *Science of the Total Environment* **2021**, 752, 141828.
39. Hagino, H.; Oyama, M.; Sasaki, S. Airborne brake wear particle emission due to braking and accelerating. *Wear* **2015**, 334-335, 44-48.
40. Hagino, H.; Oyama, M.; Sasaki, S. Laboratory testing of airborne brake wear particle emissions using a dynamometer system under urban city driving cycles. *Atmospheric Environment* **2016**, 131, 269-278.
41. Halsall, C. J.; Maher, B. A.; Karloukovski, V. V.; Shah, P.; Watkins, S. J. A novel approach to investigating indoor/outdoor pollution links: Combined magnetic and PAH measurements. *Atmospheric Environment* **2008**, 42, 8902-8909.
42. Hansard, R.; Maher, B. A.; Kinnersley, R. P. Rapid magnetic biomonitoring and differentiation of atmospheric particulate pollutants at the roadside and around two major industrial sites in the U.K. *Environmental Science & Technology* **2012**, 46, 4403-4410.
43. Harrison, R. M.; Beddows, D. C. S.; Dall-Osto, M. PMF analysis of wide-range particle size spectra collected on a major highway. *Environmental Science & Technology* **2011**, 45, 5522-5528.

44. Harrison, R. M.; Jones, A. M.; Gietl, J.; Yin, J.; Green, D. C. Estimation of the contributions of brake dust, tire wear, and resuspension to nonexhaust traffic particles derived from atmospheric measurements. *Environmental Science & Technology* **2012**, 46, 6523-6529.
45. Hoek, G.; Krishnan, R. M.; Beelen, R.; Peters, A.; Ostro, B.; Brunekreef, B.; Kaufman, J. D. Long-term air pollution and cardio-respiratory mortality: a review. *Environmental Health* **2013**, 12(43).
46. Hofman, J.; Castanheiro, A.; Nuyts, G.; Joosen, S.; Spassov, S.; Blust, R.; De Wael, K.; Lenaerts, S.; Samson, R. Impact of urban street canyon architecture on local atmospheric pollutant levels and magneto-chemical PM_{10} composition: An experimental study in Antwerp, Belgium. *Science of the Total Environment* **2020**, 712, 135534.
47. Hofman, J.; Maher, B. A.; Muxworthy, A. R.; Wuyts, K.; Castanheiro, A.; Samson, R. Biomagnetic monitoring of atmospheric pollution: A review of magnetic signatures from biological sensors. *Environmental Science and Technology* **2017**, 51, 6648-6664.
48. Hulskotte J. H. J.; Roskam, G. D.; Denier van der Gon, H. A. C. Elemental composition of current automotive braking materials and derived air emission factors. *Atmospheric Environment* **2014**, 99, 436-445.
49. Iaccarino, L.; La Joie, R.; Lesman-Segev, O. H.; Lee, E.; Hanna, L.; Allen, I. E.; Hillner, B. E.; Siegel, B. A.; Whitmer, R. A.; Carrillo, M. C.; Gatsonis, C.; Rabinovici, G. D. Association between ambient air pollution and amyloid positron emission tomography positivity in older adults with cognitive impairment. *JAMA Neurology* **2020**, DOI: 10.1001/jamaneurol.2020.3962.
50. Jang, H. Brake friction materials. In *Encyclopedia of Tribology*; Wang, Q. J., Chung, Y.-W., Eds.; Springer: New York, Heidelberg, Dordrecht, London, 2013; pp. 263-273.
51. Jeong, C.-H.; Evans, G. J.; Healy, R. M.; Jadidian, P.; Wentzell, J.; Liggio, J.; Brook, J. R. Rapid physical and chemical transformation of traffic-related atmospheric particles near a highway. *Atmospheric Pollution Research* **2015**, 6, 662-672.
52. Jung, C.-R.; Lin, Y.-T.; Hwang, B.-F. Ozone, particulate matter, and newly diagnosed Alzheimer's disease: A population-based cohort study in Taiwan. *Journal of Alzheimer's Disease* **2015**, 44, 573-584.
53. Kazimirova, A.; Peikertova, P.; Barancokova, M.; Staruchova, M.; Tulinska, J.; Vaculik, M.; Vavra, I.; Kukutschova, J.; Filip, P.; Dusinska, M. Automotive airborne brake wear debris nanoparticles and cytokinesis-block micronucleus assay in peripheral blood lymphocytes: A pilot studies. *Environmental Research* **2016**, 148, 443-449.

54. Kim, W.; Doh, S.-J.; Park, Y.-H.; Yun, S.-T. Two-year magnetic monitoring in conjunction with geochemical and electron microscopic data of roadside dust in Seoul, Korea. *Atmospheric Environment* **2007**, *41*, 7627-7641.
55. Kravchenko, J.; Darrah, T. H.; Miller, R. K.; Lyerly, H. K.; Vengosh, A. A review of the health impacts of barium from natural and anthropogenic exposure. *Environmental Geochemistry and Health* **2014**, 36, 797-814.
56. Kukutschová, J.; Filip, P. *Chapter 6 - Review of Brake Wear Emissions: A Review of Brake Emission Measurement Studies: Identification of Gaps and Future Needs*. [In:] Non-Exhaust Emissions, edited by Amato, F., Academic Press, **2018**, Pages 123-146.
57. Kukutschová, J.; Moravec, P.; Tomášek, V.; Matějka, V.; Smolík, J.; Schwarz, J.; Seidlerová, J.; Šafářová, K.; Filip, P. On airborne nano/micro-sized wear particles released from low-metallic automotive brakes. *Environmental Pollution* **2011**, 159, 998−1006.
58. Kukutschová, J.; Roubíček, V.; Malachová, K.; Pavlíčková, Z.; Holuša, R.; Kubačková, J.; Mička, V.; MacCrimmon, D.; Filip, P. Wear mechanism in automotive brake materials, wear debris and its potential environmental impact. *Wear* **2009**, 267, 807−817.
59. Kukutschová, J.; Roubíček, V.; Mašláň, M.; Jančík, D.; Slovák, V.; Malachová, K.; Pavlíčková, Z.; Filip, P. Wear performance and wear debris of semimetallic automotive brake materials. *Wear* **2010**, 268, 86−93.
60. Kumar, P.; Pirjola, L.; Ketzel, M.; Harrison, R. M. Nanoparticle emissions from 11 non-vehicle exhaust sources – A review. *Atmospheric Environment* **2013**, 67, 525-277.
61. Lamichhane, D. K.; Leem, J.-H.; Lee, J.-Y.; Kim, H.-C. A meta-analysis of exposure to particulate matter and adverse birth outcomes. *Environmental Health and Toxicology* **2015**, 30, e2015011.
62. Lawrence, S.; Sokhi, R.; Ravindra, K.; Mao, H.; Prain, H. D.; Bull, I. D. Source apportionment of traffic emissions of particulate matter using tunnel measurements. *Atmospheric Environment* **2013**, 77, 548-557.
63. Lee, P. W.; Filip, P. Friction and wear of Cu-free and Sb-free environmental friendly automotive brake materials. *Wear* **2013**, 302, 1404-1413.
64. Lehndorrf, E.; Schwark, L. Biomonitoring of air quality in the Cologne Conurbation using pine needles as a passive sampler – Part II: polycyclic aromatic hydrocarbons (PAH). *Atmospheric Environment* **2004**, *38*, 3793-3808.
65. Li, K.; Reichmann, H. Role of iron in neurodegenerative diseases. *Journal of Neural Transmission* **2016**, 123, 389-399.

66. Li, S.; Zhang, B.; Wu, D.; Li, Z.; Chu, S.-Q.; Ding, X.; Tang, X.; Chen, J.; Li, Q. Magnetic particles unintentionally emitted from anthropogenic sources: Iron and steel plants. *Environmental Science & Technology Letters* **2021**. https://doi.org/10.1021/acs.estlett.1c00164
67. Li, X.; Huang, S.; Jiao, A.; Yang, X.; Yun, J.; Wang, Y.; Xue, X.; Chu, Y.; Liu, Y.; Ren, M.; Chen, X.; Li, N.; Lu, Y.; Mao, Z.; Tian, L.; Xiang, H. Association between ambient fine particulate matter and preterm birth or term low birth weight: An updated systematic review and meta-analysis. *Environmental Pollution* **2017**, 227, 596-605.
68. Liati, A.; Schreiber, D.; Lugovyy, D.; Gramstat, S.; Dimopoulos Eggenschwiler, P. Airborne particulate matter emissions from vehicle brake in micro- and nano-scales: Morphology and chemistry by electron microscopy. *Atmospheric Environment* **2019**, 212, 281-289.
69. Liu, N.; Miyashita, L.; Maher, B. A.; McPhail, G.; Jones, C. J. P.; Barratt, B.; Thangaratinam, S.; Karloukovski, V.; Ahmed, I. A.; Aslam, Z.; Grigg, J. Evidence for the presence of air pollution nanoparticles in placental tissue cells. *Science of the Total Environment* **2021**, 751, 142235.
70. Long, X.; Luo, Y.-H.; Zhang, Z. ; Zheng, C. ; Zeng, C.; Bi, Y.; Zhou, C.; Rittmann, B. E.; Waite, T. D.; Herckes, P.; Westerhoff, P. The nature and oxidative reactivity of urban magnetic nanoparticle dust provide new insights into potential neurotoxicity studies. *Environmental Science & Technology* **2020**, 54, 10599-10609.
71. Lu, D.; Luo, Q.; Chen, R.; Zhuansun, Y.; Jiang, J.; Wang, W.; Yang, X.; Zhang, L.; Liu, X.; Li, F.; Liu, Q.; Jiang, G. Chemical multi-fingerprinting of exogenous ultrafine particles in human serum and pleural effusion. *Nature Communications* **2020**, 11, 2567.
72. Ma, J.; Olofsson, U.; Lyu, Y.; Wahlström, J.; Åström, A. H.; Tu, M. A comparison of airborne particles generated from disk brake contacts: Induction versus frictional heating. *Tribology Letters* **2020**, 68, 38.
73. Maher, B. A. Magnetic properties of some synthetic sub-micron magnetites. *Geophysical Journal* **1988**, 94, 83-96.
74. Maher, B. A. Airborne magnetite- and iron-rich pollution nanoparticles: Potential neurotoxicants and environmental risk factors for neurodegenerative disease, including Alzheimer's disease. *Journal of Alzheimer's Disease* **2019**, 71(2), 361-375.
75. Maher, B. A.; Ahmed, I. A. M.; Karloukovski, V. V.; MacLaren, D. A.; Foulds, P. G.; Allsop, D.; Mann, D. M. A.; Torres-Jardón, R.; Calderón-Garcidueñas, L. Magnetite pollution nanoparticles in the human brain. *Proceedings of the National Academy of Sciences of the United States of America* **2016**, 113(39), 10797-10801.
76. Maher, B. A.; González-Maciel, A.; Reynoso-Robles, R.; Torres-Jardón, R.; Calderón-Garcidueñas, L. Iron-rich air pollution nanoparticles: An unrecognised environmental risk

826 factor for myocardial mitochondrial dysfunction and cardiac oxidative stress. *Environmental*
827 *Research* **2020**, 188, 109816.
828 77. Maher, B. A.; Karloukovski, V. V.; Mutch, T. J. High-field remanence properties of synthetic
829 and natural submicrometre haematites and goethites: significance for environmental
830 contexts. *Earth and Planetary Science Letters* **2004**, 226, 491-505.
831 78. Maher, B. A.; Moore, C.; Matzka, J. Spatial variation in vehicle-derived metal pollution
832 identified by magnetic and elemental analysis of roadside tree leaves. *Atmospheric*
833 *Environment* **2008**, 42, 364-373.
834 79. Malachova, K.; Kukutschova, J.; Rybkova, Z.; Sezimova, H.; Placha, D.; Cabanova, K.; Filip, P.
835 Toxicity and mutagenicity of low-metallic automotive brake pad materials. *Ecotoxicology and*
836 *Environmental safety* **2016**, 131, 37-44.
837 80. Marié, D. C.; Chaparro, M. A. E.; Gogorza, C. S. G.; Navas, A.; Sinito, A. M. Vehicle-derived
838 emissions and pollution on the road Autovia 2 investigated by rock-magnetic parameters: A
839 case study from Argentina. *Studia Gephysica et Geodaetica* **2010**, 54, 135-152.
840 81. Matějka, V.; Perricone, G.; Vlček, J.; Olofsson, U.; Wahlström, J. Airborne wear particle
841 emissions produced during the dyno bench tests with a slag containing semi-metallic brake
842 pads. *Atmosphere* **2020**, 11, 1220.
843 82. Mathissen, M.; Grochowicz, J.; Schmidt, C.; Vogt, R.; Farwich zum Hagen, F. H.; Grabiec, T.;
844 Steven, H.; Grigoratos, T. A novel real-world braking cycle for studying brake wear particle
845 emissions. *Wear* **2018**, 414-415, 219-226.
846 83. Matzka, J., Maher, B. A. Magnetic biomonitoring of roadside tree leaves: identification of
847 spatial and temporal variations in vehicle-derived particulates. *Atmospheric Environment*
848 **1999**, 33, 4565-4569.
849 84. Menapace, C.; Mancini, A.; Federici, M.; Straffelini, G.; Gialanella, S. Characterization of
850 airborne wear debris produced by brake pads pressed against HVOF-coated discs. *Fristion*
851 **2020**, 8(2), 421-432.
852 85. Miller, M. R.; Raftis, J. B.; Langrish, J. P.; McLean, S. G.; Samutrtai, P.; Connell, S. P.; Wilson, S.;
853 Vesey, A. T.; Fokkens, P. H. B.; Boere, A. J. F.; Krystek, P.; Campbell, C. J.; Hadoke, P. W. F.;
854 Donaldson, K.; Cassee, F. R.; Newby, D. E.; Duffin, R.; Mills, N. L. Inhaled nanoparticles
855 accumulate at sites of vascular disease. *ACS Nano* **2017**, 11, 4542-4552.
856 86. Moreno, T.; Martins, V.; Querol, X.; Jones, T.; BéruBé, K.; Minguillón, M. C.; Amato, F.;
857 Capdevila, M.; de Miguel, E.; Centelles, S.; Gibbons, W. A new look at inhalable metalliferous
858 airborne particles on rail subway platforms. *Science of the Total Environment* **2015**, 505, 367-
859 375.

87. Muxworthy, A. R.; Matzka, J.; Davila, A. F.; Petersen, N. Magnetic signature of daily sampled urban atmospheric particles. *Atmospheric Environment* **2003**, 37, 4163-4169.
88. Muxworthy, A. R.; Schmidbauer, E.; Petersen, N. Magnetic properties and Mössbauer spectra of urban atmospheric particulate matter: a case study from Munich, Germany. *Geophysical Journal International* **2002**, 150, 558-570.
89. Nel, A.; Xia, T.; Mädler, L.; Li, N. Toxic potential of materials at the nanolevel. *Science* **2006**, 311, 622-627.
90. Noël, A.; L'Espérance, G.; Cloutier, Y.; Plamondon, P.; Boucher, J.; Philippe, S.; Dion, C.; Truchon, G.; Zayed, J. Assessment of the contribution of electron microscopy to nanoparticle characterization sampled with two cascade impactors. *Journal of Occupational and Environmental Hygiene* **2013**, 10(3), 155-172.
91. Nosko, O.; Alemani, M.; Olofsson, U. Temperature effect on emission of airborne wear particles from car brakes. *Conference Europe's Braking Conference and Exhibition* **2015**, EB2015-TEF-014.
92. Nosko, O.; Olofsson, U. Effective density or airborne wear particles from car brake materials. *Journal of Aerosol Science* **2017a**, *107*, 94-106.
93. Nosko, O.; Olofsson, U. Quantification of ultrafine airborne particulate matter generated by the wear of car brake materials. *Wear* **2017b**, 374-375, 92-96.
94. Ntziachristos, L.; Ning, Z.; Geller, M. D.; Sheesley, R. J.; Schauer, J. J.; Sioutas, C. Fine, ultrafine and nanoparticle trace element compositions near a major freeway with a high heavy-duty diesel fraction. *Atmospheric Environment* **2007**, 41, 5684-5696.
95. Oberdörster, G.; Sharp, Z.; Atudorei, V.; Elder, A.; Gelein, R.; Lunts, A.; Kreyling, W.; Cox, C. Extrapulmonary translocation of ultrafine carbon particles following whole-body inhalation exposure of rats. *Journal of Toxicology and Environmental Health, Part A* **2002**, 64, 1531-1543.
96. Oberdörster, G.; Sharp, Z.; Atudorei, V.; Elder, A.; Gelein, R.; Kreyling, W.; Cox, C. Translocation of inhaled ultrafine particles to the brain. *Inhalation Toxicology* **2004**, 16, 437-445.
97. Oudin, A.; Forsberg, B.; Nordin Adolfsson, A.; Lind, N.; Modig, L.; Nordin, M.; Nordin, S.; Adolfsson, R.; Nilsson, L.-G. Traffic-related air pollution and dementia incidence in Northern Sweden: A longitudinal study. *Environmental Health Perspectives* **2016**, 124(3), 305-312.
98. Özdemir, Ö.; Dunlop, D. J.; Moskowitz, B. M. The effect of oxidation on the Verwey transition in magnetite. *Geophysical Research Letters* **1993**, 20(16), 1671-1674.
99. Özdemir, Ö.; Dunlop, D. J. Hallmarks of maghemitization in low-temperature remanence cycling of partially oxidized magnetite nanoparticles. *Journal of Geophysical Research* **2010**, 115, B02101.

100. Pagels, J.; Gudmundsson, A.; Gustavsson, E.; Asking, L.; Bohgard, M. Evaluation of aerodynamic particle sizer and electrical low-pressure impactor for unimodal and bimodal mass-weighed size distributions. *Aerosol Science and Technology* **2005**, 39(9), 871-887.

101. Pankhurst, Q.; Hautot, D.; Khan, N.; Dobson, J. Increased levels of magnetite iron compounds in Alzheimer's disease. *Journal of Alzheimer's Disease* **2008**, 13, 49-52.

102. Pasquier, A.; André, M. Considering criteria related to spatial variabilities for the assessment of air pollution from traffic. *Transportation Research Procedia* **2017**, 25, 3354-3369.

103. Pattammattel, A.; Leppert, V. J.; Aronstein, P.; Robinson, M.; Mousavi, A.; Sioutas, C.; Forman, H. J.; O'Day, P. A. Iron speciation in particulate matter ($PM_{2.5}$) from urban Los Angeles using spectro-microscopy methods. *Atmospheric Environment* **2021**, 245, 117988.

104. Peikertova, P.; Filip, P. Influence of the automotive brake wear debris on the environment – A review of recent research. *SAE International Journal of Materials and Manufacturing* **2016**, 9(1), 133-146.

105. Peikertová, P.; Kukutschová, J.; Vávra, I.; Matějka, V.; Životský, O.; Vaculík, M.; Lee, P. W.; Filip, P. Water suspended nanosized particles released from nonairborne brake wear debris. *Wear* **2013**, 306, 89−96.

106. Perricone, G.; Alemani, M.; Metinöz, I.; Matějka, V.; Wahlström, J.; Olofsson, U. Towards the ranking of airborne particle emissions from car brakes – a system approach. *Proceedings of the Institution of Mechanical Engineers, Part D* **2017**, *231*(6), 781-797.

107. Peters, R.; Ee, N.; Peters, J.; Booth, A.; Mudway, I.; Anstey, K. J. Air pollution and dementia: A systematic review. *Journal of Alzheimer's Disease* **2019**, 70, S145-S163.

108. Plascencia-Villa, G.; Ponce, A.; Collingwood, J. F.; Arellano-Jiménez, M. J.; Zhu, X.; Rogers, J. T.; Betancourt, I.; José-Yacamán, M.; Perry, G. High-resolution analytical imaging and electron holography of magnetite particles in amyloid cores of Alzheimer's disease. *Scientific Reports* **2016**, 6(24873).

109. Pope III, C. A.; Dockery, D. W. Health effects of fine particulate air pollution: Lines that connect. *Journal of the Air & Waste Management Association* **2006**, 56(6), 709-742.

110. Puisney, C.; Oikonomou, E. K.; Nowak, S.; Chevillot, A.; Casale, S.; Baeza-Squiban, A.; Berret, J.-F. Brake wear (nano)particle characterization and toxicity on airway epithelial cells *in vitro*. *Environmental Science: Nano* **2018**, 5, 1036-1044.

111. Putaud, J.-P.; Van Dingenen, R.; Alastuey, A.; Bauer, H.; Birmili, W.; et al. A European aerosol phenomenology – 3: Physical and chemical characteristics of particulate matter from

60 rural, urban, and kerbside sites across Europe. *Atmospheric Environment* **2010**, 44, 1308-1320.

112. Radhakrishnamurty, C.; Sastry, N. P.; Deutsch, E. R. Ferromagnetic behaviour of interacting superparamagnetic particle aggregates in basaltic rocks. *Pramana* **1973**, 1(2), 61-65.

113. Rajhelová, H.; Peikertová, P.; Čabanová, K.; Kuzníková, L.; Čech Barabaszová, K.; Mamulová Kutláková, K.; Vaculík, M.; Kukutschová, J. Determination of oxidative potential caused by brake wear debris in non-cellular systems. *Journal of Nanoscience and Nanotechnology* **2019**, 19, 2869-2875.

114. Rea-Downing, G.; Quirk, B. J.; Wagner, C. L.; Lippert, P. C. Evergreen needle magnetization as a proxy for particulate matter pollution in urban environments. *GeoHealth* **2020**, 4, e2020GH000286.

115. Reed, B. E.; Yalamanchili, J.; Leach, J. B.; Hennigan, C. J. Fate of transition metals in PO_4-based *in vitro* assays: equilibrium modelling and macroscopic studies. *Environmental Science: Processes & Impacts* **2021**. DOI: https://doi.org/10.1039/D0EM00405G.

116. Roubicek, V.; Raclavska, H.; Juchelkova, D.; Filip, P. Wear and environmental aspects of composite materials for automotive braking industry. *Wear* **2008**, 265, 167-175.

117. Sagnotti, L.; Macri, P.; Egli, R.; Mondino, M. Magnetic properties of atmospheric particulate matter from automatic air sampler stations in Latium (Italy): Toward a definition of magnetic fingerprints for natural and anthropogenic PM_{10} sources. *Journal of Geophysical Research* **2006**, 111, B12S22.

118. Sagnotti, L.; Taddeucci, J.; Winkler, A.; Cavallo, A. Compositional, morphological, and hysteresis characterization of magnetic airborne particulate matter in Rome, Italy. *Geochemistry, Geophysics, Geosystems* **2009**, 10(8), Q08Z06.

119. Sagnotti, L.; Winkler, A. On the magnetic characterization and quantification of the superparamagnetic fraction of traffic-related urban airborne PM in Rome, Italy. *Atmospheric Environment* **2012**, 59, 131-140.

120. Salma, I.; Pósfai, M.; Kovácsm K.; Kuzmann, E.; Homonnay, Z.; Posta, J. Properties and sources of individual particles and some chemical species in the aerosol of a metropolitan underground railway station. *Atmospheric Environment* **2009**, 43, 3460-3466.

121. Sanders, P. G.; Dalka, T. M.; Xu, N.; Maricw, M. M.; Basch, R. H. Brake dynamometer measurements of airborne brake wear debris. *SAE Transactions* **2002**, 111(6), 1693-1699.

122. Sanders, P. G.; Xu, N.; Dalka, T. M.; Maricq, M. M. Airborne brake wear debris: Size distributions, composition, and a comparison of dynamometer and vehicle tests. *Environmental Science & Technology* **2003**, 37, 4060-4069.

123. Sanderson, P.; Delgado-Saborit, J. M.; Harrison, R. M. A review of chemical and physical characterisation of atmospheric metallic nanoparticles. *Atmospheric Environment* **2014**, 94, 353-365.

124. Sanderson, P.; Su, S. S.; Chang, I. T. H.; Delgado Saborit, J. M.; Kepaptsoglou, D. M.; Weber, R. J. M.; Harrison, R. M. Characterisation of iron-rich atmospheric submicrometre particles in the roadside environment. *Atmospheric Environment* **2016**, 140, 167-175.

125. Selley, L.; Schuster, L.; Marbach, H.; Forsthuber, T.; Forbes, B.; Gant, T. W.; Sandström, T.; Camiña, N.; Athersuch, T. J.; Mudway, J.; Kumar, A. Brake dust exposure exacerbates inflammation and transiently compromises phagocytosis in macrophages. *Metallomics* **2019**, 12, 371-386.

126. Shi, L.; Yazdi, M. D.; Braun, D.; Awad, Y. A.; Wei, Y.; Liu, P.; Di, Q.; Wang, Y.; Schwartz, J.; Dominici, F.; Koiumourtzoglou, M.-A.; Zanobetti, A. Long-term effects of $PM_{2.5}$ on neurological disorders in the American Medicare population: a longitudinal cohort study. *Lancet Planet Health* **2020**, 4(12), E557-E565.

127. Singh, N.; Jenkins, G. J. S.; Asadi, R.; Doak, S. H. Potential toxicity of superparamagnetic iron oxide nanoparticles (SPION). *Nano Reviews* **2010**, 1, 5358.

128. Smith, M. A.; Harris, P. L. R.; Sayre, L. M.; Perry, G. Iron accumulation in Alzheimer disease is a source of redox-generated free radicals. *Proceedings of the National Academy of Sciences of the United States of America* **1997**, 94, 9866-9868.

129. Spassov, S.; Egli, R.; Heller, F.; Nourgaliev, D. K.; Hannam, J. Magnetic quantification of urban pollution sources in atmospheric particulate matter. *Geophysical Journal International* **2004**, *159*, 555-564.

130. Sternbeck, J.; Sjödin, Å.; Andréasson, K. Metal emissions from road traffic and the influence of resuspension – results from two tunnel studies. *Atmospheric Environment* **2002**, 36, 4735-4744.

131. Stieb, D. M.; Chen, L.; Eshoul, M.; Judek, S. Ambient air pollution, birth weight and preterm birth: A systematic review and meta-analysis. *Environmental Research* **2012**, 117, 100-111.

132. Straffelini, G.; Ciudin, R.; Ciotti, A.; Gialanella, S. Present knowledge and perspectives on the role of copper in brake materials and related environmental issues: A critical assessment. *Environmental Pollution* **2015**, 207, 211-219.

133. Suglia, S. F.; Gryparis, A.; Wright, R. O.; Schwartz, J.; Wright, R. O. Association of black carbon with cognition among children in a prospective birth cohort study. *American Journal of Epidemiology* **2007**, 137(3), 280-286.

134. Sunyer, J.; Esnaola, M.; Alvarez-Pedrerol, M.; Forns, J.; Rivas, I.; López-Vicente, M.; Suades-González, E.; Foraster, M.; Garcia-Esteban, R.; Basagaña, X.; Viana, M.; Cirach, M.; Moreno, T.; Alastuey, A.; Sebastian-Galles, N.; Nieuwenhuijsen, M.; Querol, X. Association between traffic-related air pollution in schools and cognitive development in primary school children: A prospective cohort study. *PLoS Medicine* **2015**, 12(3), e2001792.

135. Tabner, B. J.; Mayes, J.; Allsop, D. Hypothesis: Soluble A*β* oligomers in association with redox-active metal ions are the optimal generators of reactive oxygen species in Alzheimer's disease. *International Journal of Alzheimer's Disease* **2010**, 2011, 546380.

136. Thorpe, A.; Harrison, R. M. Sources and properties of non-exhaust particulate matter from road traffic: A review. *Science of the Total Environment* **2008**, 400, 270-282.

137. Tjälve, H.; Henriksson, J.; Tallkvist, J.; Larsson, B. S.; Lindquist, N. G. Uptake of manganese and cadmium from the nasal mucosa into the central nervous system via olfactory pathways in rats. *Pharmacology & Toxicology* **1996**, 79, 347-356.

138. Verma, P. C.; Alemani, M.; Gialanella, S.; Lutterotti, L.; Olofsson, U.; Straffelini, G. Wear debris from brake system materials: A multi-analytical characterization approach. *Tribology International* **2016**, 94, 249-259.

139. Viana, M.; Kuhlbusch, T. A. J.; Querol, X.; Alastuey, A.; Harrison, R. M.; Hopke, P. K.; Winiwarter, W.; Vallius, M.; Szidat, S.; Prévôt, A. S. H.; Hueglin, C.; Bloeman, H.; Wåhlin, P.; Vecchi, R.; Miranda, A. I.; Kasper-Giebl, A.; Maenhaut, W.; Hitzenberger, R. Source apportionment of particulate matter in Europe: A review of methods and results. *Aerosol Science* **2008**, 39, 837-849.

140. Wahlström, J.; Olofsson, U. A field study of airborne particle emissions from automotive disc brakes. *Proceedings of the Institution of Mechanical Engineers, Part D: Journal of Automobile Engineering* **2014**, 229, 6.

141. Weichenthal, S.; Bai, L.; Hatzopoulou, M.; van Ryswyk, K.; Kwong, J. C.; Jerrett, M.; van Donkelaar, A.; Martin, R. V.; Burnett, R. T.; Lu, H.; Chen, H. Long-term exposure to ambient ultrafine particles and respiratory disease incidence in Toronto, Canada: a cohort study. *Environmental Health* **2017**, 16(64).

142. Wu, J.; Ding, T.; Sun, J. Neurotoxic potential of iron oxide nanoparticles in the rat brain striatum and hippocampus. *NeuroToxicology* **2013**, 34, 243-253.

143. Wu, Y.-C.; Lin, Y.-C.; Yu, H.-L.; Chen, J.-H.; Chen, T.-F.; Sun, Y.; Wen, L.-L.; Yip, P.-K.; Chu, Y.-M.; Chen, Y.-C. Association between air pollutants and dementia risk in the elderly. *Alzheimer's & Dementia: Diagnosis, Assessment & Disease Monitoring* **2015**, 1, 220-228.
144. Yang, Y.; Vance, M.; Tou, F.; Tiwari, A.; Liu, M.; Hochella Jr., M. Nanoparticles in road dust from impervious urban surfaces: distribution, identification, and environmental implications. *Environmental Science: Nano* **2016**, 3, 534-544.
145. Zhang, X.; Chen, X.; Zhang, X. The impact of exposure to air pollution on cognitive performance. *Proceedings of the National Academy of Sciences of the United States of America* **2018**, 115(37), 9193-9197.
146. Zhang, Q.; Lu, D.; Wang, D.; Yang, X.; Zuo, P.; Yang, H.; Fu, Q.; Liu, Q.; Jiang, G. Separation and tracing of anthropogenic magnetite nanoparticles in the urban atmosphere. *Environmental Science & Technology* **2020**, 54, 9274-9284.
147. Zhao, J.; Lewinski, N.; Riediker, M. Physico-chemical characterization and oxidative reactivity evaluation of aged brake wear particles. *Aerosol Science and Technology* **2015**, 49, 65-74.